Armed Services Technical Information Agency

AD

119209

UNCLASSIFIED

NOL HYPERSONIC TUNNEL NO. 4 RESULTS V
EXPERIMENTAL AND THEORETICAL INVESTIGATION
OF A COOLED HYPERSONIC WEDGE NOZZLE

13 APRIL 1953

U. S. NAVAL ORDNANCE LABORATORY

WHITE OAK, MARYLAND

NOL HYPERSONIC TUNNEL NO. 4   RESULTS V.
EXPERIMENTAL AND THEORETICAL INVESTIGATION OF
A COOLED HYPERSONIC WEDGE NOZZLE

By

P. Wegener, R. K. Lobb, E. M. Winkler,
M. Sibulkin and H. Staab

ABSTRACT: A new water cooled, wedge-type nozzle has
been in operation in the NOL 12 x 12 cm Hypersonic
Tunnel No. 4 since January 1952. This report presents
results of theoretical and experimental investigations
covering the performance of this nozzle. It was found
from measurements of pitot and static pressure that the
nozzle produced a shock-free, almost isentropic expansion
having a test-section Mach number distribution comparable
in quality to that obtained in existing conventional
nozzles at lower Mach numbers. The cooling system used
was adequate to maintain the nozzle block temperatures
at constant low values. The temperature distribution
in a nozzle block was also measured and it showed a
rise near the throat. This rise agreed qualitatively
with theoretical calculations. A comparison of the
calculated and measured rate of heat transfer to a
nozzle block suggested that boundary layer transition
occurs after the throat. A pressure and temperature
survey at the end of a nozzle block where the boundary
layer is turbulent showed that the velocity distribution
is similar to that found at low speed. This survey was
also used to calculate the overall heat transfer rate to
the nozzle block. This result agreed with that obtained
from the direct method of determining the heat transfer
by measuring the cooling water rate and temperature
increase.

In conclusion it is found that a hypersonic wedge nozzle
produces shock free expansions and acceptable flow in the
test section and serves well as a research tool.

i

NAVORD Report 2701   13 April 1953

This is the fifth NAVORD Report on an investigation
carried out in the continuous NOL 12 x 12 cm Hypersonic
Tunnel No. 4. This facility was first put into operation
in May 1950. The titles of the previous NAVORDS discussing
results from the tunnel are:

    I   Air Liquefaction. NAVORD 1742, 4 Jan 1951
    II   Diffuser Investigation. NAVORD 2376, 5 May 1952
    III   Diffuser Investigation with Models and Supports,
            NAVORD 2435, 1 July 1952
    IV   High Supply Temperature Measurement and Control,
            NAVORD 2574, 8 Oct 1952

The present NAVORD (Results V) presents an experimental
and theoretical discussion of a cooled high Mach number
nozzle. The work was jointly sponsored by the U. S. Naval
Bureau of Ordnance and the U. S. Air Force, Flight Research
Laboratory.

The authors are indebted to Messrs. Charles E. White and
E. J. Stollenwerk for the mechanical design of the nozzle.
Prof. N. Hall's advice on the cooling problem is gratefully
acknowledged. Messrs. L. Liccini and R. Garren participated
during the tests and Messrs. J. Kendall, Jr. and H. Maxwell
assisted in making the boundary layer calculations.

                        EDWARD L. WOODYARD
                        Captain, USN
                        Commander

                        H. H. KURZWEG, Chief
                        Aeroballistic Research Department
                        By direction

OUTLINE

ILLUSTRATIONS

NOL HYPERSONIC TUNNEL NO. 4   RESULTS V:
EXPERIMENTAL AND THEORETICAL INVESTIGATION OF
A COOLED HYPERSONIC WEDGE NOZZLE

INTRODUCTION

1.   During the initial planning phase (reference 1)
of the NOL 12 x 12 cm Hypersonic Wind Tunnel (Figure 1),
it was decided to use two plane blocks as a nozzle
(Figures 2 and 3) producing a continuous expansion of the
air. The Mach number in any section of such a "wedge
nozzle", and in particular, the maximum Mach number in
the exit section can then be easily varied by varying
the nozzle area ratio only. This feature appeared to be
advantageous for the study of such basic phenomena as
air condensation (reference 4), needed pressure ratios
to operate at high Mach numbers (reference 39), etc.
It was planned to later attempt the design of a nozzle
producing uniform flow in a greater region for testing
larger models. Another reason for the initial selection
of such a simple nozzle was the fact that boundary layer
corrections of theoretical potential flow nozzle walls
designed to produce such uniform flows are insufficiently
known at high Mach numbers.

2. Experimentation with two types of wedge nozzles
during the last 2-1/2 years has shown that these nozzles
produce satisfactory flow, and a theoretical and experi-
mental discussion of the nozzle performance with some
comparison with uniform flow nozzles will be given in
section II of this report.

3. To prevent air condensation in the wind tunnel at
high Mach numbers, the supply air must be preheated. Even
highly purified air does not supercool appreciably (ref-
erence 2) in contrast to the well known case of rapid
expansions of water vapor in nozzles (reference 3). It
is therefore advisable that the expansion of the air in
the tunnel does not enter the condensation region. Wind
tunnel supply temperatures and pressures for such operation
are given on Figure 8 of reference 4. Although these
temperatures are much lower than those which would simulate
actual free-flight stagnation temperatures (compare Figure 1,
reference 5), they are high enough to pose a severe

technical problem at Mach numbers above say M = 8.
At the peak Mach numbers for practicable tunnel oper-
ation, one may therefore well resort to extreme
purification to obtain some super-cooling and resultant
saving in heating as pointed out by Nagamatsu (reference 2).
In this report we will deal, however, mainly with Mach
numbers of the order 7 to 8 where a moderate supply
pressure range from 5 to 30 atmospheres at temperatures
of the order 300 to 400°C makes continuous tunnel
operation quite practical.

4. During operation at elevated supply temperatures,
all components of the tunnel are being heated by
conduction, forced convection and radiation. The nozzle
and test section walls, for example, will tend to reach
a temperature close to the recovery temperature after
some time of operation. This recovery temperature is
in turn of the order of the supply temperature. Depending
on the local rate of heat transfer from the flow, the
locally different heat capacity of the tunnel components,
etc., the equipment will become non-uniformly hot. An
example of such uneven heating of the nozzle surface and
other components is given on Figures 4 and 6 of reference 5.
It can be seen that the throat of the nozzle heats up much
more rapidly than the nozzle end (compare section V). If
supply pressure and temperature are held constant for a
fixed Mach number, one expects that finally all tunnel
components will reach some constant temperature. Such a
constant temperature could not be attained in our tunnel
after several hours of operation. On the other hand, the
slowly increasing temperatures of all tunnel components
cause warpage of metal parts, breakdown of all rubber
based seals, glass breakage, etc. Warpage is particularly
effective at the narrow nozzle throat where small area
changes result in major Mach number changes in the test
section, (see section II). In order to avoid these
difficulties, retain the flexibility of Mach number change
inherent in a two-dimensional wedge nozzle, and rapidily
attain a constant temperature and geometry, a nozzle
water-cooling system was designed and built, (Figures 1,
2 and 3). It was further found that the top of the test
section frame had to be cooled (Figure 1) to obtain fixed
base points for the nozzle bed. With such an arrangement,
the following is found (see sections II and IV):

(a) Most of the nozzle surface remains near
room temperature at all times. (In
our tunnel the cooling water discharge is
of the order 10 gallons per minute.)

(b) Constant Mach number readings in the
test section are attained after a few
minutes of operation.

(c) The tunnel can be operated continuously
for hours.

(d) Materials, gaskets, etc. do not undergo
permanent changes and all operating
conditions can be repeated accurately.

5. The following sections of this NAVORD report give
an account of some of the theoretical and experimental
work done to date on this nozzle.

II. NOZZLE DESIGN AND PERFORMANCE

6. **Design Problems of Hypersonic Nozzles.** The aero-
dynamic design of a potential flow nozzle for Mach
numbers above 5.0 is the same as that for conventional
supersonic nozzles. There are several methods (all
based on theory of characteristics) for determining
the contours of both two and three-dimensional nozzles.
A two-dimensional nozzle can be designed by the graphical
method of Prandtl and Busemann (reference 6) or by the
semi-graphical method given by Puckett (reference 7 and 8).
These methods are tedious and are subject to graphical
error especially in the hypersonic range for which the
characteristic net becomes greatly elongated. The
analytical methods of Foelsch (reference 9) and Atkin
(reference 10) are usually preferred for practical reasons
because they are more accurate and can be used on high
speed computing machines. In the three-dimensional case
the design is complicated by the fact that the characteristic
net in the hodograph plane has to be determined step by
step along with the net in the physical plane. However,
for axially symmetric flows there are available several
graphical, numerical and analytical methods (see references
11, 12 and 13). A three-dimensional nozzle of arbitrary
cross-section can be obtained by tracing the stream lines
that outline the area throughout a known axially symmetric
flow (see references 14 and 15). This method has the
disadvantage that the cross-sectional shape so obtained

varies along the nozzle thus making it difficult to
fabricate. It may be possible to correct the surfaces
to give a constant cross-sectional shape by a linearized
method of characteristics such as given by Ferri in
reference 16. Another type of three-dimensional nozzle
employing a square throat and expanding in two stages,
first in one plane then in the plane at right angles,
is described in reference 17.

7. One of the main practical problems in hypersonic
nozzle design is the achievement of a smooth flow through
the nozzle throat. For high Mach numbers the ratio of
the test section area to throat area becomes very large.
As a result for medium sized tunnels the throat must be
a narrow slit or some configuration of equivalent area.
This is illustrated in the table below. The throat
must therefore be machined very accurately. The
mechanical design is further complicated by the possible
warpage of the throat due to the high surface temperatures

TABLE II-I

Throat and Exit Areas for Two and Three-Dimensional ($M = 8$) Nozzles.

Nozzle	Test Area		Throat Area
Two-dimensional		12 x 12 cm	.063 x 12 cm
Axially Symmetric		12 cm dia.	.87 cm dia.
Square throat and exit plane		12 x 12 cm	.87 x .87 cm

that can occur in this region during "hot" tunnel operation
(see section IV and V). Also the subsonic section must
usually withstand high pressures while in the supersonic
portion the pressure is very low. (The NOL hypersonic
tunnel no. 4 operates at supply pressures up to 30 atm).
High supply pressures are required in order to have
continuum flow in the test section at high Mach numbers.

8. A two-dimensional nozzle was selected for the NOL hypersonic tunnel for the following reasons. (1) Nozzle boundary-layer corrections are not accurate at high Mach numbers (primarily due to the lack of skin-friction data, see reference 15). In the two-dimensional case the boundary layer can be allowed for approximately, by adjusting the nozzle blocks. For an axially symmetric or square nozzle, on the other hand, errors in the boundary-layer correction resulting in poor Mach number distribution, would require remachining the surfaces or discarding the nozzle. (2) Disturbances in an axially symmetric nozzle tend to focus along the axis. (3) A two-step, three-dimensional nozzle is unsatisfactory (see reference 17) because of boundary-layer affects. (4) The cost of fabricating a three-dimensional nozzle is considerably higher than for a two-dimensional nozzle.

9. For the initial tests in the hypersonic tunnel a two-dimensional wedge nozzle (straight diverging walls) was chosen in preference to a uniform flow nozzle. With this wedge nozzle a wide range of Mach numbers can be achieved by simply changing the throat opening without introducing disturbances due to incorrect nozzle contour. The flow in a hypersonic wedge nozzle, for small wall angles, closely approximates two-dimensional source flow (constant properties along circular arcs with centers roughly at the throat). In a uniform flow nozzle, on the other hand, the flow expands slowly along the nozzle walls as compared to that along the axis. This produces relatively strong "cross-flow" pressure gradients which cause the boundary layer on the sidewalls to build up along the centerline (references 19 and 20). Also a wedge nozzle of the same length and Mach number, as a uniform flow nozzle, has a smaller maximum wall angle. This reduces the possibility of flow separation.

10. Previous investigations in a minimum length uniform flow nozzle designed for $M = 5.18$ have shown that a small radius at the throat can lead to such flow separation and shock waves (see Figure 4). Here the throat radius is about 1/16" and the wall angle slightly downstream of the throat is $36.2°$. In order to minimize this effect, the throat of the wedge nozzle was formed as a cylinder of 3/8" radius and the wall angle was kept to approximately $5-1/2°$. Shadowgraph and schlieren photographs of the flow near the throat of the wedge nozzle for a Mach number setting of 5.0 are given in Figure 5. (This setting corresponds to the

largest throat opening possible with the present nozzle).
From these photographs we can see that there is no
separation or large disturbances in the flow field. The
triangular pattern appearing in the schlieren photograph
agrees roughly with that found graphically by the method
of characteristics. The distortion of the throat in the
shadowgram is optical and is due to the large density
gradients in this region of flow.

11. When the tunnel is operated at high supply temperatures
the nozzle blocks become heated and tend to expand, par-
ticularly in the throat region where the rate of heat
transfer is large. The expansion is inward because the
tunnel casing, to which the blocks are attached, remains
relatively cold. As a result the throat area decreases
and the nozzle exit Mach number increases with time. By
introducing a cooling system (see Figures 1, 2 and 3) the
nozzle dimensions can be kept constant after a short period
of operation (For $p_o = 10$ atm, $T_o = 593°K$ and $M = 7.0$ the
nozzle blocks reach equilibrium after about ten minutes of
operation). The sensitivity of Mach number to coolant rate
is illustrated in Figure 6. It can be seen that without
any nozzle cooling the Mach number increases with time.
Nozzle cooling also tends to keep the boundary-layer
characteristics constant with time.

12. Flow Calibration. An example of the flow calibration
will be given for a Mach number of 7.0 only. However, the
results are generally true for other Mach number settings
This particular setting corresponds to that chosen for the
boundary-layer survey and the heat-transfer measurements
given in sections III and IV.

13. The flow in a plane 1" upstream from the nozzle exit
was surveyed with pitot and static pressure probes. Static
pressures along the centerline of the nozzle sidewall were
also measured. The pitot probes were made from .095"
hypodermic tubing with a wall thickness of .01". The static
pressure probes were made from the same tubing with an 8°
cone attached to the tip. Four .025" orifices were located
20 probe diameters aft of the shoulder. The static orifices
in the nozzle sidewall had an opening of 025". In order
to measure the low static pressures near the nozzle exit
(of the order of 2mm Hg) it was necessary to use a silicone
oil micro-manometer equipped with an optical reading system.
This instrument has an accuracy of better than 1/2% in the

range under consideration. A precision mercury manometer
or calibrated aneroid type gauges were used for measuring
the higher pitot pressures.

14. A plot of the static pressure distribution along
the centerline of the nozzle sidewall in terms of the
supply pressure, for an exit Mach number of 7.0, is given
in Figure 7. There appears to be a smooth expansion along
the entire length of the nozzle. The pressure gradient at
the nozzle exit corresponds to a drop in Mach number of
about .02 M/cm. This compares with the value of .03 M/cm
derived from one-dimensional theory assuming inviscid
flow throughout the nozzle in which case the growing
boundary layer on the nozzle wall is neglected.

15. The Mach number distribution for various traverses
in a plane 1" upstream from the nozzle exit as determined
from pitot and static pressure measurements at the identical
location using the Rayleigh formula are given in Figure 8.
The maximum variation in Mach number, outside of the
boundary layer, is 2%. In earlier surveys it was found that
there were disturbances in the flow origination near the
junctions of the nozzle throat with the sidewalls. By
using metal to metal seals between the nozzle and sidewalls
these disturbances could be practically eliminated as
indicated by the smooth Mach number distributions. From
these measurements we find the stagnation pressure loss
throughout the nozzle to be about 4%. A schlieren
photograph of the flow in the nozzle exit for a Mach number
of 7.0 is given in Figure 5.

16. Boundary-Layer Growth. If at some station along the
nozzle the Mach number in the free stream is known then
we can estimate the boundary-layer displacement thickness
on the nozzle walls by comparing the flow area obtained
from isentropic flow tables with the geometrical area
enclosed by the walls. (A one-dimensional analysis is
sufficient here since it closely approximates the two-
dimensional analysis for a wall angle of only 5-1/2°.)
In the calculations we assume that the boundary layer is
of equal thickness on all four walls and zero at the
throat (in section V the displacement thickness is shown
to be about .005 mm at the throat). Also since the
stagnation pressure loss in this nozzle is small, we can
determine the flow area with good accuracy from simply
the ratio of the static pressure to the supply pressure
using isentropic flow tables. Therefore, for each static
pressure measurement on the nozzle sidewall we can obtain

a displacement thickness. The growth of the boundary
layer displacement thickness along the nozzle obtained
in this manner is compared to that calculated by Tucker's
method (reference 18) in Figure 9. In the theory the
walls are assumed to be thermally insulated, whereas the
actual nozzle walls are cooled. This probably accounts
for the experimental values being thinner (i.e. increased
density near the wall) than those calculated by the
theory. The displacement thickness determined directly
from the boundary-layer survey (see section III) fits
well with the other experimental points. It is interesting
to note that the total thickness of the boundary layer at
the nozzle exit obtained by Tucker's method is 24 mm
which is close to the 26 mm measured in the boundary layer
survey.

III. TURBULENT BOUNDARY-LAYER CHARACTERISTICS AT END OF NOZZLE

17. In addition to the indirect determination of
growth of the displacement thickness along the nozzle
wall discussed in the last section, a detailed survey
of the boundary-layer profiles at one point was undertaken.
A survey was made perpendicular to the west nozzle wall one
inch from the nozzle exit. The data were unaffected by the
juncture of nozzle end and first diffuser plates. Since
the position of the transition point along the nozzle is still
unknown, it is interesting to note that at this survey station
a fully developed turbulent boundary layer was found. The
pertinent results are summarized in the following table.

TABLE III: Boundary-Layer Survey

Station: Center of west nozzle wall, 1" upstream of
nozzle exit.
Supply pressure: p_o = 10 atmospheres
Supply temperature: T_o = 593°K (50° above that temperature
needed to avoid air condensation
throughout.)
Wall temperature at survey station: T_w = 316°K (cooling
system in operation)
Free stream temperature: T_∞ = 56°K (T_w/T_∞ = 5.7)
Free stream Mach number: M_∞ = 7.0 ± 0.01
Free stream velocity: u_∞ = 1040 m/sec
Free stream Mach number gradient: Appr. 0.02 M/cm (compare
section II)

Reynolds number based on displacement thickness:
$$Re\ (\delta^*) = 43,000$$
Re based on equivalent flat plate length (calculated):
$$Re\ (x) \simeq 10^7$$
Boundary-layer thickness at point where $u = 0.995\ u_\infty$,
$$\delta = 26\ mm$$
Displacement thickness: $\delta^* = 10.5$ mm
Momentum thickness: $\theta = 1.24$ mm
Energy thickness (see section V): $\phi = 2.78$ mm.

18. The above data were taken in the following manner:
Static pressure was measured by a hole 1/2 mm diameter
in the wall and by a 5° cone-cylinder static probe in
the free stream just outside the edge of the boundary
layer. (Silicone oil manometers of about ± 2 microns
measuring accuracy during tunnel operation were used.)
Since agreement between these two static pressure was
found to be of the order of 1 per cent, a constant value
of static pressure was assumed to exist through the
boundary layer.

19. Pitot pressure was surveyed from wall to free stream
with a flattened hypodermic tube of about 0.18 mm opening.
This opening is large enough to avoid errors due to slip
flow effects on the impact pressure measurement in the
region of low Reynolds numbers in the boundary layer near
the wall (reference 21).

20. From measured pitot pressure and static pressure,
the local Mach number could be determined from the
Rayleigh formula (reference 8 p. 95). The Rayleigh Mach
number is shown on Figure 10a. (The assumption of the
validity of the perfect gas law implicit in this evaluation
and the use of $\gamma = 1.4$ is warranted in our range of
thermodynamic data (reference 22, Figure 19). The distance
from the wall y, is made dimensionless by the boundary-
layer thickness $\delta = 26$ mm. At the measured point closest
to the wall ($y = 0.1$ mm), the flow is still supersonic
($M \simeq 1.3$).

21. Total temperature was surveyed with a shielded,
total temperature probe. This probe was calibrated in
the free stream in approximately the range of Mach numbers,
densities and temperatures encountered in the boundary-
layer measurements. The probe recovery factor

$$r = \frac{T_i - T_\infty}{T_0 - T_\infty} \qquad (III,1)$$

9

is smaller than one because of instrumental errors due
to radiation and conduction from the thermocouple junction
to the surroundings. Such errors are particularly hard
to overcome at the high Mach numbers (low test section
density) and high temperatures (large radiation losses)
in question. Using the measured free stream recovery
factor to correct the boundary-layer total temperature
measurement, we obtain Figure 10b. The measurement
closest to the wall was at $y = 2$ mm. A linear total
temperature distribution was assumed between this point
and the measured wall temperature. From the measured
Mach number and total temperature, the static temperature
can be computed using the energy equation in the form

$$T = \frac{T_o'}{\frac{\gamma-1}{2}M^2 + 1} \tag{III,2}$$

22. Finally the velocity profile may be calculated
employing the definition of Mach number $M = u/a = u/\sqrt{\gamma RT}$
and obtaining

$$\frac{u}{u_\infty} = \frac{M}{M_\infty}\sqrt{\frac{T}{T_\infty}} \tag{III,3}$$

This velocity profile is shown in Figure 10c which includes
the results of four independent runs. A 1/7 - power
profile is indicated for comparison.

23. Since all flow properties in the boundary layer are
now known, the integrands in the equations defining
displacement, momentum and energy thickness, (see section
VI), could now be calculated and plotted. The integrals
themselves were determined using a planimeter. The results
are given in Figure 10 and Table III,2. Comparing these
ratios to those given by the estimates of either Tucker
(references 18 and 35) or Eckert (reference 24) for the
insulated flat plate case at the same M_∞, we find the
following qualitative effects of heat transfer to the wall:

TABLE III,2

$M_\infty = 7$

	Measured Case: $T_w/T_\infty = 5.7$	Estimate (reference 18 or 24), assuming insulated flat plate; $Pr = 1$, 1/7 - power profile and $T_w/T_\infty = 10.8$.
δ^*/δ	.4	.61
θ/δ	.05	.027

The direction of deviation of the measured values
from those derived theoretically is expected from
the increased density near the wall in the experi-
mental case with heat transfer. (Cooling of the wall
has an effect qualitatively somewhat similar to suction.)

24. The Reynolds number based on free stream conditions
and displacement thickness is 43,000. On the other hand
an estimate of an equivalent flat plate Reynolds number
was made assuming that free stream conditions of the
survey station would have prevailed outside the boundary
layer of an equivalent flat plate. Using the incompress-
ible formula for boundary-layer thickness as function of
Reynolds number or that obtained by Eckert (reference 24,
equation 37) for a compressible case with unaltered
velocity profile and no heat transfer, we obtain a flat
plate Reynolds number of the order 10^7. Conversely, our
survey station would correspond to that taken on a plate
with a turbulent boundary layer of about 1.5 m length
and our free stream condition. Our small tunnel may then
be taken to simulate conditions in a large tunnel capable
of operating with a flat plate model of such length
successfully, if the small pressure gradient and previous
boundary-layer history do not affect a fully developed
turbulent boundary layer.

25. In section IV it will be seen that the temperature
in the steel nozzle blocks drops linearly with distance
from the surface after a steady state of supply conditions
and cooling system operation has been reached. The time
history of such a measurement is shown on Figure 18. A
cut parallel to the T - axis through this figure at some
time produces plots of temperature distribution like that
given on Figure 19. Since the heat conductivity of the
nozzle material is known, the rate of heat transfer per
unit area at the boundary-layer station could be determined
from

$$q = k \frac{dT}{dy} . \tag{III,4}$$

On the other hand the heat transfer coefficient is defined by

$$q = h(T_e - T_w) . \tag{III,5}$$

26. We could now determine the Stanton number (some-
times called dimensionless heat transfer coefficient $c_{h\infty}$)
from

$$St_\infty = \frac{h}{c_p \rho_\infty u_\infty} = \frac{k(dT/dy)}{c_p \rho_\infty u_\infty (T_e - T_w)} , \quad \text{(III,6)}$$

if we knew the insulated flat plate temperature, T_e.
However, since $T_e \cong T_o \cong 600^\circ K$, we were not able
to measure its value at present. We therefore calculated
St_∞ in two ways. First we take the known approximate
expression for the turbulent recovery factor (reference 29)
$r = \sqrt[3]{P_r}$. We then choose $P_r = 0.73$ based upon
thermodynamic properties near the wall and obtain $T_e = 539^\circ K$
and $St_\infty = 0.00075$. Secondly by using $P_r = 1$ (and thus
$T_e = T_o = 593^\circ K$), we obtain $St_\infty = 0.00061$.

27. To obtain the local friction coefficient we apply
the relation (given in reference 26, equation 20).

$$Nu_\infty = \frac{C_f \sqrt{Re_\infty}}{2} \sqrt{Re_\infty} \sqrt[3]{P_r} , \quad \text{(III,7)}$$

which may be transformed into

$$\frac{C_f}{2} = St_\infty P_r^{2/3} \quad \text{(III,8)}$$

Using (III,8) we obtain numerically $C_f = 0.0012$ for both
combinations of P_r and T_e discussed above. We now calculate
the shear stress at the wall

$$\tau_w = C_f \frac{\rho_\infty}{2} u_\infty^2 . \quad \text{(III,9)}$$

28. Finally, it is possible to use this value for the
representation of the velocity profile in the parameters

$$u^+ = \frac{u}{\sqrt{\frac{\tau_w}{\rho_w}}} , \quad \text{and} \quad y^+ = \frac{y\sqrt{\frac{\tau_w}{\rho_w}}}{\nu_w} \quad \text{(III,10)}$$

(reference 27). These parameters are based on wall
density and kinematic viscosity since this plot is of

greatest interest near the wall. Figure 3 shows our
measurement with the region based upon interpolated
total temperature data given as a dashed line. For
comparison, von Karman's incompressible flow semi-
logarithmic law (reference 27) and assumed linear
velocity distribution ($u^+ = y^+$) in the laminar
sublayer are shown. Finally a compressible flow
profile calculated from equation 72 of van Driest's
analysis (reference 25) for our M_∞ and T_w/T_∞ is
given. Aside from other assumptions inherent in
van Driest's analysis, the calculated profile has the
boundary condition $u = u_\infty$ at $y = \delta$, matching
the measured profile at this point.

29. Summarizing, it may be stated that the boundary-
layer characteristics near the nozzle exit are quite
similar to those encountered in incompressible turbulent
boundary layers. Although the heat transfer to the wall
does not affect the velocity distribution materially, it
alters the relative magnitudes of displacement and momentum
thickness with respect to the insulated flat plate case.
Finally, one cannot discern a laminar sublayer from our
data possibly because we were unable to take total
temperature measurements in that range which is roughly
coincident with the estimated extent of the incompressible
laminar sublayer.

IV. MEASUREMENT OF SURFACE TEMPERATURES
AND TOTAL HEAT TRANSFER

30. Any experiments to determine recovery temperatures,
heat transfer data, and many other types of investigations
rely upon the accuracy with which the wind-tunnel supply
temperature, T_0, is known. The correct reference T_0 is
assured if the supply temperature is uniform and constant
over practically the entire nozzle inlet cross-section.
The achievement of such conditions, Figure 12, was there-
fore a prerequisite to the experiments described in the
following (reference 28).

31. Due to design (cooling system) and operational range
(high M, high T_0) of the hypersonic tunnel, experimental
arrangements to obtain wall surface temperatures or
overall heat transfer data have to be different from those
used at other places (reference 29). There is some

question about the precision that can be obtained if
surface temperatures are measured with a temperature
gradient in the nozzle wall induced by the nozzle
cooling system. However. the results obtained show
that practically steady-state conditions are reached
within a few minutes after starting a tunnel run, and
that errors due to conduction and radiation are probably
of the same order of magnitude as the experimental
scatter of the data.

32. Measurement of Surface Temperature. With the
nozzle cooled by a measured rate of water flow through
the cooling system (see section IX), a steady-state
temperature distribution will be established in the
nozzle wall. This distribution is a function of the
temperature, pressure, Mach number, coolant flow, etc.
of the tunnel operation. Depending on these variables
and the amount of preheating done through the by-pass,
it will take some time until practically steady-state
temperatures are attained. If there are no serious
non-uniformities in the wall material, no strong
temperature gradients in the nozzle in the z-direction,
and if the nozzle wall can be practically treated as a
slab of fixed dimensions, then the temperature in the
nozzle wall will drop linearly with distance from the
nozzle surface. By measuring the temperatures at
various depths, it should then be possible to obtain
surface temperatures by linear extrapolation. In this
fashion one avoids the insertion of measuring elements
that may disturb the flow on the nozzle surface.

33. Temperatures of the nozzle wall can be measured
at any of 13 points along the center line of each nozzle
block with four thermocouples imbedded into the nozzle
wall at various depths from the surface, (see Figure 2).
To make installation and exchange of this arrangement
more convenient, the thermocouples were inserted in
separate plugs (see Figure 34). These plugs were ground
to fit appropriate holes in the nozzle wall. With the
plugs made of the same material as the nozzle wall, it
is assumed that they do not cause a greater disturbance
of the temperature field than does the presence of the
thermocouples itself. To reduce conduction errors along
the thermocouple wires in the plugs, they are led for a
certain length behind the junction parallel to the nozzle
surface, in the direction of the z-axis.

34. The e.m.f. output of the thermocouples is measured with Brown temperature recorders (model 153X11P28A1)[1] (Superscripts refer to the list in section VIII) or a K-2 type Leeds and Northrup[2] potentiometer, depending upon the temperature difference across the nozzle wall and the accuracy required. With the Brown recorders the temperature of the individual points can be read to $\pm 0.3^{\circ}C$ (reference 28). Using the K-2 type potentiometer wall temperatures and/or wall temperature differences can be read consistently to within $0.01^{\circ}C$ during actual operation of the tunnel.*

35. Most of the tests described here were made with the cooling rate adjusted to 6.5 gallons per minute per nozzle block. With this rate practically steady-state readings are achieved in a few minutes. (A change of this cooling rate just gives a displacement of the temperature level.) In this case the cooling water passed through two passages near the throat (Figure 2). One passage at the nozzle exit was partially open and all the remaining ones were closed. Measurements of surface temperature at $M_s = 7.6$ given here as example cover the temperature range $340^{\circ}K \leq T_0 \leq 615^{\circ}K$ (Figure 13) and the pressure range $9 \text{ atm} \leq p_0 \leq 15 \text{ atm}$, (Figure 14). These measurements were taken near the nozzle throat and it can be seen that in all cases the nozzle surface temperature (distance $= 0$ cm) is considerably below the tunnel supply temperature and equal to or slightly higher than room temperature. An increase in supply pressure (Figure 14) and in supply temperature (Figure 13) causes an increase of the steady-state nozzle surface temperature due to the increased rate of heat transfer for a fixed rate of coolant flow. Measurements at given p_0 and T_0 at nine stations along the center line of the

---

*This accuracy requires the use of selected, calibrated thermocouple wire, same wire material from hot junction to ice bath, Cu-wire from ice bath to potentiometer and galvanometer (i.e. the same as used within these instruments), careful and repeated balancing of the potentiometer circuit, achieved with Leeds and Northrup standard cell and a Willard constant potential storage battery), and finally a stable reference ice bath.

nozzle surface (Figures 15 and 16) were evaluated to
extrapolate nozzle surface temperatures, wall temperature
gradients (Figures 15 and 16) and to construct isothermes
through the nozzle wall, (Figure 17). Finally measure-
ments of wall temperatures at the boundary-layer survey
station (see Figure 2) were repeated with higher precision
using the K-2 type potentiometer. The results indicate a
slow increase of the temperature at each thermocouple
location with time, (Figure 18). This is possibly due
to the fact that exact steady-state conditions cannot be
reached, as long as radiative heat transfer from the un-
cooled sidewalls whose temperature increases slowly
during the test is present. However, the fact that this
temperature change is only about $0.7^{\circ}K$ in 3/4 hours permits
us to consider operation as practically stationary.

36   Assuming no longitudinal heat conduction in the
nozzle wall, complete insulation of the nozzle block from
sidewall and test section frame (a fact that is very
nearly true), absence of radiation effects, etc.,
temperature-depth curves such as shown may be used to
determine the local rate of heat transfer. (The rate
of local heat transfer per unit area is given by the
product of heat conductivity of the material times the
temperature gradient) (see equation III,4). Figure 19 is
a cross-plot of Figure 18 averaged for 10 different
abscissa values to eliminate the small time effect. With
$k_{steel} = 50.4$ kcal/h m $^{\circ}K$ and $\Delta T/\Delta y = 48.1$ $^{\circ}K/m$ from
Figure 19, we find a local rate of heat transfer per
unit area q $= 2424 \pm 73$ kcal/m^2 hr at the boundary-layer
survey station ($M_\infty = 7$). This rate of heat transfer
at the test section is very low in contrast to the throat
region, mainly due to the low test section density.
(Compare e.g. the heat output of 675 kcal/m^2 h from a
steam radiator under standard conditions, i.e. room
temperature $24^{\circ}C$, steam temperature $110^{\circ}C$, reference
30, p. 91).

37. Tests to determine the total rate of heat transfer
require again a constant p_o, a constant and uniform T_o
and a steady-state temperature distribution across the
nozzle walls. The quantities to be measured are the
coolant rate, the temperature of the incoming or outgoing
coolant, and the temperature increase of the coolant.
The cooling rate is measured with a Flowrator, (see section
IX), after the coolant pressure is equalized in the lines
to both nozzle blocks. The temperature of the incoming

COOLING RATE (GALLONS/MIN)	WATER TEMPERATURE INCREASE (^{o}K)	HEAT FLOW RATE ($6.27 \times 10^{-2} \times \Delta T \times$ COOLING RATE) (10^{3} KCAL/HR)
$M_S = 8.0 \quad p_o = 20$ ATM $\quad T_o = 600^{o}$K		
$6.6 \pm 0.8\%$	$1.50 \pm 0.5\%$	2.25 ± 0.054
$6.5 \pm 0.9\%$	$1.50 \pm 0.5\%$	2.23 ± 0.054
$5.3 \pm 0.9\%$	$1.84 \pm 0.6\%$	2.20 ± 0.036
$5.2 \pm 1.0\%$	$1.89 \pm 0.8\%$	2.22 ± 0.040
$3.9 \pm 0.8\%$	$2.47 \pm 0.8\%$	2.17 ± 0.036
$3.8 \pm 0.9\%$	$2.55 \pm 0.7\%$	2.19 ± 0.036
$2.6 \pm 1.9\%$	$3.50 \pm 0.6\%$	2.07 ± 0.050
$2.5 \pm 0.8\%$	$3.68 \pm 0.9\%$	2.04 ± 0.036
$1.4 \pm 1.5\%$	$6.30 \pm 0.6\%$	1.92 ± 0.040
$M_S = 7.6 \quad p_o = 10$ ATM $\quad T_o = 593^{o}$K		
$6.3 \pm 2.3\%$	$0.92 \pm 2.2\%$	1.32 ± 0.06

TABLE I-IV   SUMMARY OF RESULTS OF TOTAL HEAT
TRANSFER MEASUREMENTS

and outgoing water is measured in the center of the inlet duct and in the center of both outlet ducts, respectively, with 30 gauge I.C. thermocouples. The thermocouples are immersed into the water for about 2.5 cm, with the unsupported portions coated with Glyptal and sealed into the support. Because of the range of temperature differences involved (order of 1° to $10^\circ C$), the thermocouple e.m.f. is measured with the K-2 type potentiometer. Measurements at various cooling rates, 1.5 gallons/min to 6.5 gallons/min per nozzle block, were made for $M_B = 8.0$ and $p_c = 20$ atm, $T_0 = 600^\circ K$ (Figure 20) the conditions for which the heat transfer will be calculated in the next chapter. The results are given in Figure 21 and Table I.

38. The errors given in Table I are those resulting from the scatter of the experimental data. Estimates show that in comparison to them errors due to conductive and radiative heat transfer to and from the nozzle surface and surrounding boundaries can probably be neglected. The nozzle blocks are well insulated from most of the surrounding metal parts by an air space, silicone rubber seals, and only a small band of metal-to-metal contact. (The temperature gradient across the metal-to-metal contact is comparable to that existing in the subsonic part of the nozzle, see Figure 17). Conduction errors are therefore believed to be negligibly small. Radiative heat transfer from the uncooled tunnel walls can also be neglected if the walls are kept smooth and unoxidized. For an order of magnitude estimate of the error we assume a pessimistic case where the sidewalls of the tunnel over their entire lengths are at supply air temperature while the nozzle walls are kept at room temperature. We assume further that the total energy radiated from the sidewalls is transferred to the nozzle neglecting the geometry. Using $Q_{rad} = A \sigma \varepsilon (T_1^4 - T_2^4)$ (reference 31, p. 215), with $A = 360$ cm^2 for the sidewall area, the Stefan-Boltzmann constant $\sigma = 1.37 \times 10^{-12}$ cal/sec cm^2 $^\circ K^4$, $T_{sidewall} = 600^\circ K$, $T_{nozzle} = 300^\circ K$, we obtain Q_{rad} of 22 kcal/hr if the emittance of the sidewalls is 0.1. This upper bound of the radiative heat transfer from the sidewall to the nozzle surface amounts to only about 1 per cent of the total measured heat transfer across the nozzle wall, (Table I), and may therefore be neglected.

V. THEORETICAL HEAT TRANSFER CALCULATIONS AND COMPARISON WITH MEASUREMENTS

39. Since the air flowing through the tunnel is heated and the nozzle walls are cooled, there is a continual flow of heat from the air, through the nozzle wall, into the cooling water. A steady-state heat transfer analysis can be applied to this problem (see section IV). This analysis can be subdivided into the following parts.

    (a) The heat transfer by forced convection from a high velocity, compressible fluid to a plane wall.

    (b) The flow of heat by conduction in a homogeneous solid of a particular geometry.

    (c) Forced convection to water flowing through tubes.

    (d) The transfer of heat by radiation from the uncooled sidewalls to the nozzle walls.

The amount of heat transferred by (d) may be neglected (see section IV).

A. Overall Heat Transfer

40. If we assume that there are effective adiabatic planes midway between the transverse cooling passages (Figure 22) and that all the heat which enters the nozzle wall in the length ΔL is removed by the cooling water, the overall heat transfer can be defined by the equation

$$q = UA_w\left(T_e - T_c\right) \qquad (V,1)$$

Furthermore, we have

$$\frac{1}{UA_w} = \frac{1}{h_c A_c} + \frac{b}{h_e A_w} + \frac{1}{h_d A_w} \qquad (V,2)$$

from, for example, reference 32, page 136. The quantities on the right-hand side of equation $(V,1)$ represent respectively the resistance to heat flow of

the cooling water, the nozzle wall, and the air stream; they are discussed in detail below.

41. Heat transfer to cooling water. The heat transferred to the cooling water per unit area of nozzle surface is given by

$$\frac{q}{A_w} = \frac{A_c}{A_w} h_c \left(T_b - T_c\right) \qquad (V,3)$$

In calculating h_c we assume

(a) that the entire surface of the cooling passage is at the same temperature T_b,

(b) that the temperature rise of the water is small enough to neglect the change of u, k, and Pr with temperature, and

(c) that the water flow is turbulent (true for our Reynolds numbers). We select the heat-transfer correlation based upon experimental results for turbulent flow through smooth pipes suggested in reference 32, page 167.

$$N_u = 0.24 R^{0.8} P_r^{0.4} \qquad (V,4)$$

Substituting the following values of fluid properties taken at 14°C (the temperature of our cooling water)

$\mu = 1.15 \times 10^{-3}$ kg/sec m,
$k = 1.40 \times 10^{-4}$ kcal/sec x °K, and
$D = .00792$ m

in equation (V,4) gives

$$h_c = 7.60 \, W_c^{0.8} \qquad (V,5)$$

It should be noted that in equation (V,5) W_c refers to the weight of water entering the center of the nozzle block (see section X-X, Figure 3). Half of this water flows through each side of the cooling passage.

Substituting equation (V,5) into equation (V,3) with $\Delta L = 0.0190$ m gives

$$\frac{q}{A_w} = 10.0\, W_c^{0.8}\left(T_b - T_c\right) \qquad (V,6)$$

42. Heat conduction in nozzle wall. The heat transferred through a homogeneous wall of constant thickness is given by

$$q = \frac{k\, A\, \Delta T}{x} \qquad (V,7)$$

By analogy the heat transferred through the nozzle wall can be formally defined as

$$q = k\, \frac{k_e}{k}\, \frac{A_w}{b}\left(T_w - T_b\right) \qquad (V,7a)$$

where the effects of the coolant tube size and position on the heat flow pattern in the wall are put into an "effective conductivity" k_e. Assuming the cooling passage to act as a heat sink and using the method of images, N. Hall found that for this particular case

$$\frac{k}{k_e} = \frac{\Delta L}{2\pi b}\, \ln\left[\frac{\sinh\sqrt{\left(\pi D/2\Delta L\right)^2 + \left(2\pi b/\Delta L\right)^2}}{\sinh\left(\pi D/2\Delta L\right)}\right] \qquad (V,8)$$

Equation (V,8) is shown graphically in Figure 23. In our nozzle $b = 0.0159$ m and from Figure 23, $k/k_e = 0.925$. It is sufficiently accurate to use a mean value of k. Selecting 440°K as a mean wall temperature gives $k = 0.012$ kcal/sec m $^{\circ}$K, and substituting these values into equation (V,7a) gives

$$\frac{q}{A_w} = 0.825\left(T_w - T_b\right) \qquad (V,9)$$

43. Heat transfer from air to nozzle wall. The heat transferred to the nozzle wall is defined as

$$\frac{q}{A_w} = h_a\left(T_e - T_w\right) \qquad (V,10)$$

The calculation of h_a is a major problem in itself and will be considered in detail later on.

44. Equations (V,6), (V,9), and (V,10) giving
alternative expressions for q can be considered a
system of three equations in the three unknowns q,
T_w, T_b and could be solved analytically for particular
values of T_e, T_c, W_c and h . Alternatively, a graphical
form of trial-and-error solution using Figure 24 may be
more useful since it is usually quicker than an analytical
solution and gives a better feeling for the effects of
changes in the values of the parameters. To use this
graph a value of q is assumed and, for the prescribed
values of W_c and h_a, this fixes $T_e - T_w$, $T_w - T_b$, and
$T_b - T_c$. The sum of these three temperature differences
must equal the prescribed $T_e - T_c$. If they do not, a
new value of q is chosen and the procedure repeated
until agreement is reached.

B. Calculation of h_a

45. The calculation of h_a must be based upon the use
of the boundary-layer concept,i.e. the effects of heat
transfer to the walls are confined to the portion of air
flowing near the walls leaving a core of air in the center
of the tunnel having the pressure and temperature corre-
sponding to an isentropic expansion from supply conditions.
Unfortunately, it has not been possible to experimentally
determine the point of transition from a laminar to a
turbulent boundary layer in our wedge nozzle. It is
known that the boundary layer at the exit of the nozzle
is turbulent (see section III); however, the strong
favorable pressure gradient and the extraction of heat
from the boundary layer are likely to delay transition
(reference 33), and it is quite possible that the boundary
layer is laminar at the throat. For these reasons,
calculations will be made assuming either a laminar or a
turbulent boundary layer throughout for a typical case
$M_s = 8.0$, $p_o = 20$ atm., and $T_o = 600^{\circ}K$.

46. The velocity distribution along the edge of the
boundary layer is given with sufficient accuracy by
assuming one-dimensional flow based upon the geometric
area (see section II). This velocity distribution is
shown in Figure 25 together with an outline of the nozzle
walls. It can be seen that most of the velocity change
takes place near the throat. This is shown again by
plotting the local value of air acceleration along the
nozzle (Figure 26); the peak value is approximately 10^7 g's.

47. The simplest approach to the boundary-layer problem
is to neglect the pressure gradient (and any temperature
gradient) along the nozzle. The nozzle is then hypo-
thetically divided into sections, each of which has a
different but constant velocity to which the flat plate
(i.e., zero pressure gradient) boundary-layer laws are
applied. This was done by calculating local values of
Reynolds number along the nozzle. The length used in
computing the Reynolds number was measured from the
nozzle inlet screen (the point shown as 0 meters in
Figure 25). The local skin friction coefficients were
found from

$$c_f = 0.664 \, Re^{-1/2} \text{ (laminar)}$$

or

$$c_f = 0.059 \, Re^{-1/5} \text{ (turbulent)}$$

depending upon the type of flow assumed. The heat
transfer was then assumed to be given by the modified
Reynolds' analogy (see paragraph 27)

$$St \, P_r^{2/3} = \frac{c_f}{2} \qquad (V,11)$$

where St is based upon free-stream conditions. The
heat transfer coefficient can now be found from

$$h_a = St \, c_p \rho u = St \, P_r^{2/3} \frac{c_p (\rho u)^*}{P_r^{2/3}} \frac{A^*}{A} \qquad (V,12)$$

Using equation (V,11), $c_p = 0.247$ kcal/kg $^\circ$C and Pr $= 0.68$
(for $t^* = 500^\circ$K),

$$h_a = 2130 \, c_f \frac{A^*}{A} \qquad (V,13)$$

is obtained. Since A*/A varies much more rapidly with
distance along the nozzle then c_f, the heat transfer
coefficient will have its maximum value near the nozzle
throat (since A*/A is greatest at M = 1). This is shown
in the graphs of h_a vs. x, assuming either turbulent or
laminar flow, given in Figures 27 and 28. Since the value
of h_a given by equation (V,13) approaches infinity as x
approaches 0, it was felt that as our initial point was
chosen somewhat arbitrarily it would be undesirable to use
equation (V,13) too near it. Instead the value of h_a from

$x = 0$ to $x = 0.016$ m ($M = 0.01$) was arbitrarily taken
as the value at the latter point. This is also done
on all subsequent graphs of h_a vs. x.

48. Because the analysis given above does not consider
the effects of longitudinal pressure gradients on the
growth of the boundary layer and on h_a, its validity
near the nozzle throat (where there is a strong pressure
gradient) is doubtful. For this reason further cal-
culations were made by methods which include some of
the effects of pressure gradients. Again separate
calculations were made assuming either a completely
laminar or completely turbulent boundary layer.

49. In both cases the methods used were based upon
the momentum - integral equation (reference 34).

$$\frac{d\theta}{dx} + \left[\frac{H+2}{u_\infty} \frac{du_\infty}{dx} + \frac{1}{\rho_\infty} \frac{d\rho_\infty}{dx} \right] \theta = \frac{\tau_w}{\rho_\infty u_\circ^2} \qquad (V,14)$$

For the laminar boundary layer the method of Howarth
(reference 35) as modified by Low (reference 36) was
used. This method is based upon the assumption of a
one parameter family of boundary-layer velocity profiles
using the Pohlhausen parameter λ which is a function
of the local boundary layer thickness and pressure
gradient. Since in our case, values of λ larger than
the maximum given in reference 36 were obtained, the
method was extended using some of the results given by
Thwaites (reference 37). Low's analysis also includes
the following assumptions: (a) constant T_o' across the
boundary layer (the result of assuming zero heat transfer
and $Pr = 1$, (b) $\mu/\mu_\infty = C\ (T/T_\infty\ )$, and (c) constant
T_w along the nozzle surface (implied by assumption (a)).
Since this method involved a changing velocity profile,
both the growth of θ with x and the value of τ_w for a
given θ are affected by the value of the local pressure
gradient. Equations (V,11) and (V,12) were used to
compute h_a since no better relation exists between heat
transfer and skin friction for compressible flow. The
variation of θ and h_a with x assuming laminar flow is
shown in Figures 29 and 30.

50. For the assumption of turbulent flow, the method
of Tucker (reference 38) was used. In this analysis a

constant boundary-layer profile given by the power
law

$$\frac{u}{u_\infty} = \left(\frac{y}{\delta}\right)^{\frac{1}{N}} \tag{V,17}$$

is used, and the skin friction is assumed as

$$\frac{\tau_w}{\rho u^2} = \frac{0.0131}{Re^{1/7}} \tag{V,18}$$

The length Reynolds number along the nozzle surface is
of the order of 10^6, and consequently a value of $N = 7$
was used. In equation (V,18), ρ and Re were based
upon stagnation temperature. Since reference 38 assumes
zero heat transfer and a "turbulent Prandtl number" equal
to 1, T_0' is constant across the boundary layer and equal
to T_0. The tabulated values given in reference 38 begin
at $M = 0.1$. For the initial growth of the boundary layer
where $M < 0.1$ an incompressible form of the momentum
integral equation was used. Assuming

$$\frac{d\rho_\infty}{dx} = 0 . \quad H = \frac{9}{7} \quad \text{and} \quad \frac{\tau_w}{\rho_\infty u_\infty^2} = \frac{0.0252}{\left(\frac{u_\infty \theta}{\nu_\infty}\right)^{1/4}}$$

and integrating equation (V,14) gives

$$\theta^{5/4} = \frac{0.0157 \, \nu_\infty^{1/4}}{u_\infty^{4.11}} \int_0^x u_\infty^{3.86} dx + \left(\frac{u_{\infty 0}}{u_\infty}\right)^{4.11} \theta_0^{5/4} \tag{V,19}$$

from which the growth of the boundary layer can be
computed (the subscript 0 referes to conditions at the
chosen initial point). Since θ_0 appears only in the
last term of equation (V,19), it is evident that since
$u_{\infty 0}/u_\infty$ decreases rapidly downstream of the starting
point (see Figure 25), the effect of the initial value
of θ becomes negligible. This means that the calculated
thickness of the boundary layer at the nozzle throat
is practically independent of the assumed distance
from the throat to the boundary-layer starting point. The
values of h_a were again computed using equations (V,11)

and (V,12). The variation of θ and h_a with x assuming turbulent flow is shown in Figures 31 and 32.

51. **Boundary-layer thickness at nozzle throat.** It should be noted that despite our small nozzle throat opening (equal to 0.025" at $M_g = 8.0$) the boundary layer at this point is still relatively thin. Assuming turbulent flow, the calculation of paragraph 50 gives

$$\frac{2 \times \delta^* \text{ (throat)}}{\text{throat opening}} = \frac{2 \times 0.00016}{0.025} = 0.013$$

52. All the heat-transfer coefficient distributions which have been calculated are shown in Figure 32 where they can be more easily compared. The average heat-transfer coefficient $\bar{h}_a$ has been calculated for each case, and the values are tabulated in Table V-I together with the maximum value of h_a (in units of kcal/sec m^2 $^\circ K$). The value of $\bar{h}_a$ is important in determining the overall

TABLE V-I

Case	$\bar{h}_a$	h_a (max.)
Laminar with pressure gradient	0.033	2.0
Laminar without pressure gradient	0.0091	0.18
Turbulent with pressure gradient	0.067	3.3
Turbulent without pressure gradient	0.060	1.5

cooling requirements for the nozzle, while the maximum value of $\bar{h}_a$ is important in determining the maximum temperature on the nozzle surface. In some cases the maximum surface temperature (which occurs very near the throat) may be more of a design limitation than the overall cooling load. It can be seen from Table V-I that including the effect of pressure gradients in the laminar boundary-layer case triples $\bar{h}_a$ and multiplies h_a (max.) by ten.

In the turbulent boundary-layer case, including the
effect of pressure gradients doubles h_a (max.) but
only increases $\bar{h}_a$ slightly.

C. Estimation of T_w at Nozzle Throat

53. The nozzle surface temperature T_w could now be
calculated using Figure 24 and the values of h_a found
in the preceding section. Near the throat, however, h_a
varies rapidly while Figure 24 is based upon having a
constant value of h_a over the length ΔL. Nevertheless,
conservative estimates of T_w at the throat (in the sense
of giving too high a value of T_w) have been made using
the four values of h_a (max.) previously calculated. The
calculation is also conservative because it neglects the
conduction of heat in the nozzle wall parallel to the
surface away from the maximum temperature point. The
calculation was made for $T_e = 587^{O}K$ (based upon a recovery
factor of 0.88), $T_c = 287^{O}K$, and $W_c = 3$ gal/min (the
estimated coolant flow rate through the cooling passages
on each side of the throat; see section IV). The computed
values of T_w and T_b at the nozzle throat are shown in
Table V-II.

TABLE V-II

Case	T_w (^{O}K)	T_b (^{O}K)
Laminar with pressure gradient	516	341
Laminar without pressure gradient	354	303
Turbulent with pressure gradient	538	346
Turbulent without pressure gradient	497	337

Except for the assumption of laminar flow without
pressure gradient, Table V-II shows that most of the
temperature drop takes place in the steel nozzle block.

D. Comparison of Calculated Values of Heat Transfer
    with Measurements.

54. Using the measured nozzle surface temperature
(see section IV) and the estimated values of T_w at
the throat, the rate of heat transfer to the nozzle
block can be calculated from

$$Q = \bar{h}_a \, A \, \overline{(T_e - T_w)} \tag{V,20}$$

where $\overline{T_e - T_w}$ is an average temperature difference
along the nozzle surface. For a coolant flow rate of
6.5 gal/min a value of $\overline{T_e - T_w}$ equal to 225°K was used
(where T_e is based upon a recovery factor of 0.88).
The values of Q calculated from equation (V,20) and
the measured value of Q (Figure 21) to one nozzle block
for a coolant rate of 6.5 gal/min per nozzle block are
shown in Table V-III.

TABLE V-III

Case	Q (kcal/sec)
Laminar with pressure gradient	0.58
Laminar without pressure gradient	0.16
Turbulent with pressure gradient	1.2
Turbulent without pressure gradient	1.0
Experimental value	.62

It can be seen that the calculated value of Q based
upon the assumption of a completely laminar boundary
layer and including the effects of pressure gradients
is closest to and lower than the measured value. This
is the condition which should prevail if transition
from a laminar to a turbulent boundary layer occurred

several centimeters downstream of the nozzle throat
since the difference in heat transfer between laminar
and turbulent flow downstream of such a transition
point would be small compared to the heat transfer
from the laminar boundary-layer upstream of the point.

E. Estimation of Heat Transfer Rate from Boundary-
Layer Measurements.

55. It is interesting to note that an estimate of
the total heat transfer rate to the nozzle walls for
$M_s = 7.6$, $p_0 = 10$ atm., and $T_0 = 593^\circ$K can be obtained
from the boundary-layer measurements given in section
III. This heat transfer rate can then be compared
with the value (given in section IV) obtained from the
cooling water temperature rise for the same conditions.
Consider the growth of a boundary layer from stations
1 to 2 as shown in the sketch below.
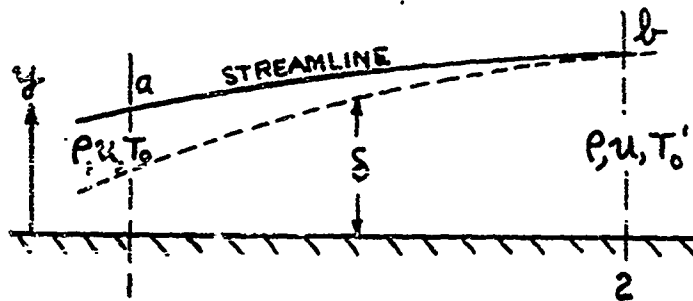
It is assumed that the streamline $\overline{ab}$ is always outside
of the velocity and temperature boundary layers. It is
also assumed that T_0' is constant and equal to T_0 across
the boundary layer at station 1, and that c_p is constant.
From the conservation of energy law, the heat transfer Q
to the wall between stations 1 and 2 must equal the
difference in the energy flowing past station 1 and
station 2,

$$Q = w c_p T_0 \int_0^a \rho_1 u_1 \, dy - w c_p \int_0^b \rho_2 u_2 (T_0')_2 \, dy \quad (V,21)$$

but from the continuity law

$$\int_0^a \rho_1 u_1 \, dy = \int_0^b \rho_2 u_2 \, dy \quad (V,22)$$

combining equations (V,21) and (V,22) gives

$$Q = w c_p \int_0^b \rho_2 u_2 \left[T_0 - (T_0')_2 \right] dy \qquad (V,23)$$

Equation (V,23) can be used to define an energy thickness ϕ such that

$$Q = w c_p \left(\rho_\infty u_\infty \right)_2 \left(T_0 - T_{w_2} \right) \phi_2 \qquad (V,24)$$

where

$$\phi_2 = \int_0^b \left(\frac{\rho u}{\rho_\infty u_\infty} \right)_2 \left[\frac{T_0 - (T_0')_2}{T_0 - T_{w_2}} \right] dy$$

In applying equation (V,24) to our nozzle, station 1 was taken at the nozzle inlet and station 2 at the boundary-layer measurement station 1 inch upstream of the nozzle exit. The heat transferred to the 1 inch portion of the nozzle block downstream of this station is negligible compared to the total. A more serious error of undetermined magnitude results from neglecting the variation of T_0 across the nozzle inlet station. Consequently, the value of Q obtained must be considered approximate. A comparison of Q (for one nozzle block) obtained from equation (V,24) and the value of ϕ measured in section III, and from the cooling water temperature rise (see section IV) is shown in table V-IV.

TABLE V-IV

Type of Measurement of Heat Transfer Rate	Q(kcal/sec)
Boundary-layer energy deficiency	0.33
Cooling water temperature rise	0.36

The agreement between these two measurements is probably within the experimental accuracy.

VI. Notation

A	flow area
A_c	surface area of coolant tube ($= \pi D_w$)
A_w	nozzle surface area per coolant tube ($= \Delta L \times w$)
b	perpendicular distance from nozzle surface to center of coolant tube
c_f	local skin-friction coefficient
c_p	specific heat at constant pressure
D	diameter of coolant tube
h_a	local heat-transfer coefficient for the air
h_c	heat-transfer coefficient for the coolant
$\bar{h}_a$	average air heat-transfer coefficient ($= \frac{1}{L} \int_0^L h_a \, dx$)
$\bar{H}$	equals δ^*/θ
k	thermal conductivity
k_e	"effective thermal conductivity" defined by Eq. (V,8)
L	length
ΔL	distance along nozzle surface between "effective adiabatic planes" (See Fig. 22)
M	Mach number
M_s	nozzle Mach number setting
Nu	Nusselt number ($= hL/k$)
p	static pressure
p_0	supply pressure
p'_0	pitot pressure (in supersonic flow the stagnation pressure behind a normal shock)

Pr	Prandtl number ($= c_p \mu / k$)
q	rate of heat transfer per unit area
Q	rate of heat transfer
r	recovery factor ($= \left[T_w - T_\infty \right] / \left[T_0 - T_\infty \right]$)
R	gas constant
Re	Reynolds number ($= \rho ux / \mu$)
St	Stanton number ($= h / \rho u c_p$)
T	static temperature
T_0	supply temperature ($\simeq$ free stream stagnation temperature)
T_0'	local stagnation temperature
T_i	temperature indicated by stagnation temperature probe (uncorrected)
T_e	equilibrium temperature (also called recovery temperature)
T_b	coolant tube surface temperature
T_c	coolant temperature
u	velocity
w	nozzle width
W_c	weight flow rate of coolant
x	distance in flow direction
y	distance perpendicular to flow direction
γ	ratio of specific heats
δ	boundary-layer thickness
δ^*	boundary-layer displacement thickness ($= \frac{1}{\rho_\infty u_\infty} \int_0^\infty (\rho_\infty u_\infty - \rho u) \, dy$)
Θ	boundary-layer momentum thickness ($= \frac{1}{\rho_\infty u_\infty^2} \int_0^\infty \rho u (u_\infty - u) \, dy$)

μ	viscosity
ν	kinematic viscosity
ρ	density
τ	shear stress
ϕ	boundary-layer energy thickness (defined by Eq. (V, 24)

Subscripts

w	at the nozzle surface
∞	in the free stream

Superscripts

*	at $M = 1$

VII. REFERENCES

1. Wegener, Peter P., Investigation of Possible Air Condensation in the Supersonic Wind Tunnel at High Mach Numbers, NOLM 8659, August 1946

2. Willmarth, W. W. and Nagamatsu, H. T., Condensation of Nitrogen in a Hypersonic Nozzle, Journ. of Appl. Phys. 23, 10 October 1952, p. 1089

3. Oswatitsch, K., Die Nebelbildung in Windkanaelen und ihr Einfluss auf Modellversuche. Jahrbuch. Deutsch. Luftf. Forsch. 1941

4. Wegener, Peter P., Stollenwerk, E., Reed, S.. and Lundquist, G., NOL Hyperballistics Tunnel No. 4 Results I: Air Liquefaction, NAVORD Report 1742, January 1951

5. Wegener, Peter P., High Temperature Operation of Hypersonic Wind Tunnels, Bureau of Ordnance Symposium on Aeroballistics, May 1952, Pasadena, California

6. Prandtl, L. and Busemann, A., Naherungsverfahren zur zeichnerischen, Ermittlung von ebenen Stroemungen mit Geschwindigkeit. Stodola Festschrift, Zurich, 1929 p. 499

7. Puckett, A. E., Supersonic Nozzle Design, Jour. Appl. Mech. 13, 4 December 1946

8. Ferri, A., Elements of Aerodynamics of Supersonic Flows, Macmillan, New York, 1949

9. Foelsch, K., A New Method of Designing Two-Dimensional Laval Nozzles for a Parallel and Uniform Jet, North American Aviation Report NA-46-235-2, May 1946

10. Atkin, A. O. L., Two-Dimensional Supersonic Channel Design, Part I, A.R.C.R & M No. 2174, 1945

11. Sauer, R., Method of Characteristics for Three-Dimensional Axially Symmetrical Supersonic Flows, NACA TM 1133, January 1947

12. Isenberg, J. S., The Method of Characteristics
    in Compressible Flow, Part 1, Air Material
    Command Rep. F-TR-1173A-ND, December 1947

13. Foelsch, K., The Analytical Design of an Axially
    Symmetric Laval Nozzle for a Parallel and Uniform
    Jet, Jour. Aero. Sci., 16, 3 March 1949

14. Evvard, J. C. and Maslen, S. H., Three-Dimensional
    Supersonic Nozzles and Inlets of Arbitrary Exit
    Cross Section, NACA TN 2688, June 1952

15. Beckwith, I. E., Ridyard, H. W. and Cromer, N.,
    The Aerodynamic Design of High Mach Number Nozzles
    Utilizing Axisymmetric Flow with Application to
    a Nozzle of Square Test Section, NACA TN 2711,
    June 1952

16. Ferri, A., The Linearized Characteristics Method
    and its Application to Practical Non-Linear
    Supersonic Problems, NACA TN 2515, October 1951

17. McLellan, C. H., Williams, T. W., and Bertram, M. H.,
    Investigation of a Two-Step Nozzle in the Langley
    11 inch Hypersonic Tunnel, NACA TN 2171, September 1950

18. Tucker, M., Approximate Calculation of Turbulent
    Boundary-Layer Development in Compressible Flow,
    NACA TN 2337, April 1951

19. Bollay, W., Aerodynamics of Supersonic Aircraft
    and Missiles, NOLR 1131, 1949

20. Haefeli, R. C., Use of Fences to Increase Uniformity
    of Boundary Layer on Side Walls of Supersonic Wind
    Tunnels, NACA RM E52E19, 1952

21. Kane, E. D. and Maslach, G. J., Impact-Pressure
    Interpretation in a Rarefied Gas at Supersonic Speeds,
    NACA TN 2210, October 1950

22. Wegener, Peter P., On the Experimental Investigation
    of Hypersonic Flow, NOLM 9629, July 1948

23. Burcher, M., Compressible Flow Tables for Air,
    NACA TN 1592, August 1948.

24. Eckert, H. U., Characteristics of the Turbulent
Boundary Layer on a Flat Plate in Compressible
Flow from Measurements of Friction in Pipes,
Jour. Aero. Sci. 17, 9 September 1950

25. Van Driest, E. R., Turbulent Boundary Layer in
Compressible Fluids, Jour. Aero. Sci. 18,
3 March 1951

26. Johnson, H. A. and Rubesin, M. W., Aerodynamic
Heating and Convective Heat Transfer - Summary
of Literature Survey, Trans. ASME, 71, 5, p. 447,
1949

27. Von Karman, Th., Turbulence and Skin Friction,
Jour. Aero. Sci. 1, 1, January 1934

28. Winkler, E. M., NOL Hypersonic Tunnel No. 4
Results IV: High Supply Temperature Measurement
and Control, NAVORD Report 2574, October 1952

29. Kaye, J., Keenan, J. H., Klingensmith, K. K.,
Ketchum, G. M. and Toong, Tau-Yi, Measurement of
Recovery Factors and Friction Coefficients for
Supersonic Flow of Air in a Tube, MIT Technical
Report No. 6418-3, May 1951

30. Allen, J. R., Walker, J. H., and James, J. W.,
Heating and Air Conditioning, McGraw-Hill, New York
1946

31. Eckert, E. R. G., Introduction to the Transfer of
Heat and Mass, McGraw-Hill, New York 1950

32. McAdams, W. H., Heat Transmission, McGraw-Hill,
2nd edition, 1942

33. Lees, L., The Stability of the Laminar Boundary
Layer in a Compressible Fluid, NACA TR 876, 1947

34. Goldstein, S., Modern Developments in Fluid Dynamics,
1st edition, pp. 131-133, 1938

35. Howarth, L., Concerning the Effect of Compressibility
on Laminar Boundary Layers and Their Separation,
Proceedings of the Royal Society, A-194, p. 16, 1948

36. Low, G. M., Simplified Method for Calculation of
    Compressible Laminar Boundary Layer with Arbitrary
    Free-Stream Pressure Gradient, NACA TN 2531, 1951

37. Thwaites, B., Approximate Calculation of the
    Laminar Boundary Layer, Aeronautical Quarterly, 1,
    p. 245, 1949

38. Tucker, M., Approximate Turbulent Boundary-Layer
    Development in Plane Compressible Flow Along
    Thermally Insulated Surfaces with Application to
    Supersonic Tunnel Contour Correction, NACA TN 2045,
    1950

39. Wegener, Peter P., Lobb, R. K., An Experimental
    Study of a Hypersonic Wind-Tunnel Diffuser, Jour.
    Aero. Sci. 20, 2, p. 105, February 1953

VIII. LIST OF MANUFACTUERES

1. Brown Instrument Co.,
    4539 Wayne Avenue
    Philadelphia 44, Pennsylvania

2. Leeds & Northrup
    4901 Stenton Avenue
    Philadelphia 44, Pennsylvania

                          Manufactured by:
3. Potomac Rubber Co.,   Connecticut Hard Rubber Co.,
    1421 H Street, N. W.   407 E Street
    Washington, D. C.   New Haven 9, Connecticut

4. Johns Manville Co.,
    22 E. 40th Street
    New York 16, N. Y.

5. Fisher & Porter Co.,
    Hatboro,
    Pennsylvania

6. General Electric Corporation
    Schenectady 5,
    New York

7. V-B Ames C.,
    Fremont,
    Ohio

8. Bausch and Lomb Optical Co.,
    Rochester,
    New York

IX. APPENDIX

Construction of Nozzle and Cooling System

1. The nozzle blocks shown in Figures 1 and 2 were machined from a solid block of steel purchased under the Navy Department Specification 46 S1J-Grade M. This material has the following chemical composition: 0.31% carbon, 0.25% Mn, 0.045% P, 0.055% Si, 0.35% Cu and 0.25% Ni. The finish machining of the surfaces of the nozzle in contact with the flow was accomplished by surface grinding parallel to the centerline of this surface. The surfaces were made flat to within 0.00025 inches, and smooth within an average of 16 RMS (root-mean-square) micro inches measured perpendicular to the nozzle centerline or flow direction and 5 RMS micro inches parallel to nozzle centerline. The inlet or subsonic portion and the .375 inch throat radius portion were ground perpendicular to the nozzle using a contour-shaped wheel. During this operation the nozzle blocks were set up side-by-side so that each cut would traverse both blocks; thus producing identical throat radii. During this set-up the nozzle alignment surface was ground, thus providing means for accurate alignment of the nozzles with respect to each other when installed in the tunnel. After grinding, final polishing of the throat was done by hand to produce a 5 RMS micro inch finish. Particular care was taken so that there would be no irregularity at the line of tangency of the supersonic plane surface and the throat radius.

2. The method of aligning and supporting the nozzle is shown in Figure 1. The nozzle clamping linkage, which is actuated by a jackscrew mechanism at its lower end, is geometrically arranged such that it exerts one major force component on the nozzle in the vertical direction to seat the nozzle against its upper alignment surface, and another component to set it firmly on its 4 adjustable legs. Alignment of the nozzle crosswise of the case is controlled by two alignment pins which protrude from the bottom surface of the nozzle and engage in slots in the case.

3. The change of Mach number setting is accomplished by adjusting the two screw type legs nearest the nozzle throat using feeler gage stock in either side of the

nozzle throat. The final throat is measured with
vernier calipers graduated to one thousandth of an
inch. The accuracy of the throat setting is within
0.0005 inches by checking with a series of feeler
gages using a "go and no'go" system. The accuracy
of the final opening measurement of the nozzle is no
better than 0.003 inches because of the wedge angle
of the nozzle and the human error of locating
repeatably the final opening.

4. The dimension of the gasket grooves, as shown
below were determined to both retain the gasket
material and to allow the door to close to a metal-
to-metal seat while affecting a seal.
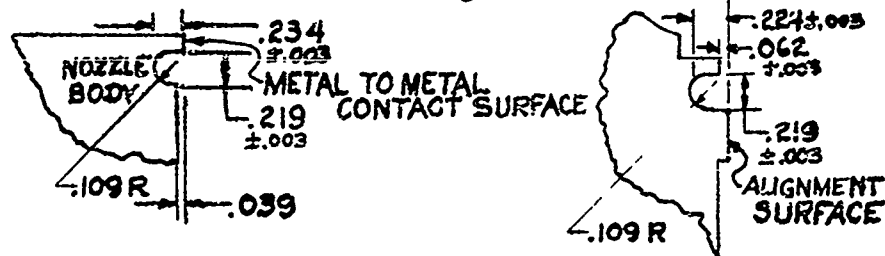
NOZZLE GASKET GROOVE   GASKET GROOVE BETWEEN
  PARALLEL TO FLOW   NOZZLE BODY & TUNNEL CASE

The gasket material used throughout the tunnel is
"Cohrlastic Silicone Rubber R-8925"[3] which was purchased
in 1/4 inch diameter extruded cord form. The best
tolerance available on the diameter is ± .015 inches,
to this date.

5. A portion of the tunnel that is intimately
associated with the cooling wedge nozzle is the air
supply inlet system, (reference 28), Figure 12. This
arrangement consists of a baffle system followed by a
honeycomb in an insulated chamber for mixing the air to
obtain a nearly uniform temperature distribution ahead
of the nozzle throat. A stainless steel screen in a
"transite"[4] frame was found desirable to prevent clogging
of the throat and probes by foreign particles, chips of
the ceramic insulators and oxide flakes, from the exposed
elements of the electric heaters. This system produces
a nearly uniform supply temperature at the nozzle throat.

Cooling System

1. The internal cooling passage arrangement of the
nozzle block, as shown in Figure 3, consists of a
central inlet-water-distribution passage with 34 holes
of 0.312 inch diameter located 5/3 inches from the
air-flow surface. These holes connect this inlet
passage to each of the two side outlet passages and
can be easily closed (e.g. by removal of the side
plates and stopping the holes with rubber cord), or
restricted by insertion of an orifice plate.

2. The exterior piping arrangement, as shown in
Figure 1, is made up of standard 1 inch copper water
tubes. The water supply main is located beneath the
floor on the lower left. It is controlled by a valve
attached to a removable "T" handle (not shown). The
water is fed to the right side of the tunnel through
the tube near the floor on the far side of the tunnel.
The inlet water pressure was equalized by the right-
angle valves and the rate of flow is measured, in the
nozzle under study by a variable area type flow Meter[5]
on the intake pipe shown at left. The two exhaust
water pipes coming from each nozzle converge and join
immediately outside of the tunnel. The flow from each
nozzle is throttled separately by valves located at
the level of the circular window on the far side of
the tunnel.

3. The coolant used is tap water. For the usual
flow rate of 6.5 gallons per minute the inlet water
pressure is 6.5 psi and the outlet pressure is
throttled to maintain a pressure of 1 psi.

Thermocouple installation

1. The nozzle temperatures are measured by iron-
constantan thermocouples made of #30 gage wire[2] and
electric welded without flux using a Variac and Pyrotip
burner[6] with a carbon electrode. The thermocouples
were secured in place using technical "B" copper cement[7]
in a modified taper pin, shown in Figure 34. The exact
location of each of the four thermocouple junctions in

each plug is determined to 0.01 millimeters after
assembly by use of a tool maker's microscope[8] (Bausch
and Lomb - Type UK 352). Special care is taken in
the manufacture of the plugs so that each plug would
bottom in its respective hole in the nozzle block.

Plug #	1	2	3	4	5	6
Location from Final Nozzle Opening (Inches)	.656	1.406	4.406	7.406	9.656	11.906

7	8	9	10	11	12	13
14.156	16.406	18.656	20.156	21.656	23.156	24.156

TUNNEL SIDEWALLS

1. Several door arrangements are available for the tunnel.
There is one set of blank steel doors, one steel door
with 42 centerline pressure taps located one inch apart,
a set of doors having a rectangular plate glass window,
and a set of doors having 3 circular windows (see window
in Figure 1). The pressure tap door and the circular
window doors are provided with two sets of hinge arms
so that when the door is inverted the tap holes and
windows bisect their former location. The circular
windows now in use are cut from selected commercial
plate glass. Experience indicates, that while running
at supply temperatures of 900°F these windows can be
used anywhere from the nozzle exit through the diffuser
for a maximum period of 20 minutes without fracture.
A fused quartz window of similar arrangement is now
being tested to increase the time of exposure.

2. When the doors are closed they are forced by bolting
against the raised nozzle lips, which forms the edges of
flow surface and against the metal-to-metal bearing
surface, of the tunnel case (see Figure 1 outside of
gasket). In addition to bolting around the periphery,

the doors are reinforced in the high pressure region,
by a rectractable bar and jackscrew arrangement (shown
in Figure 1).
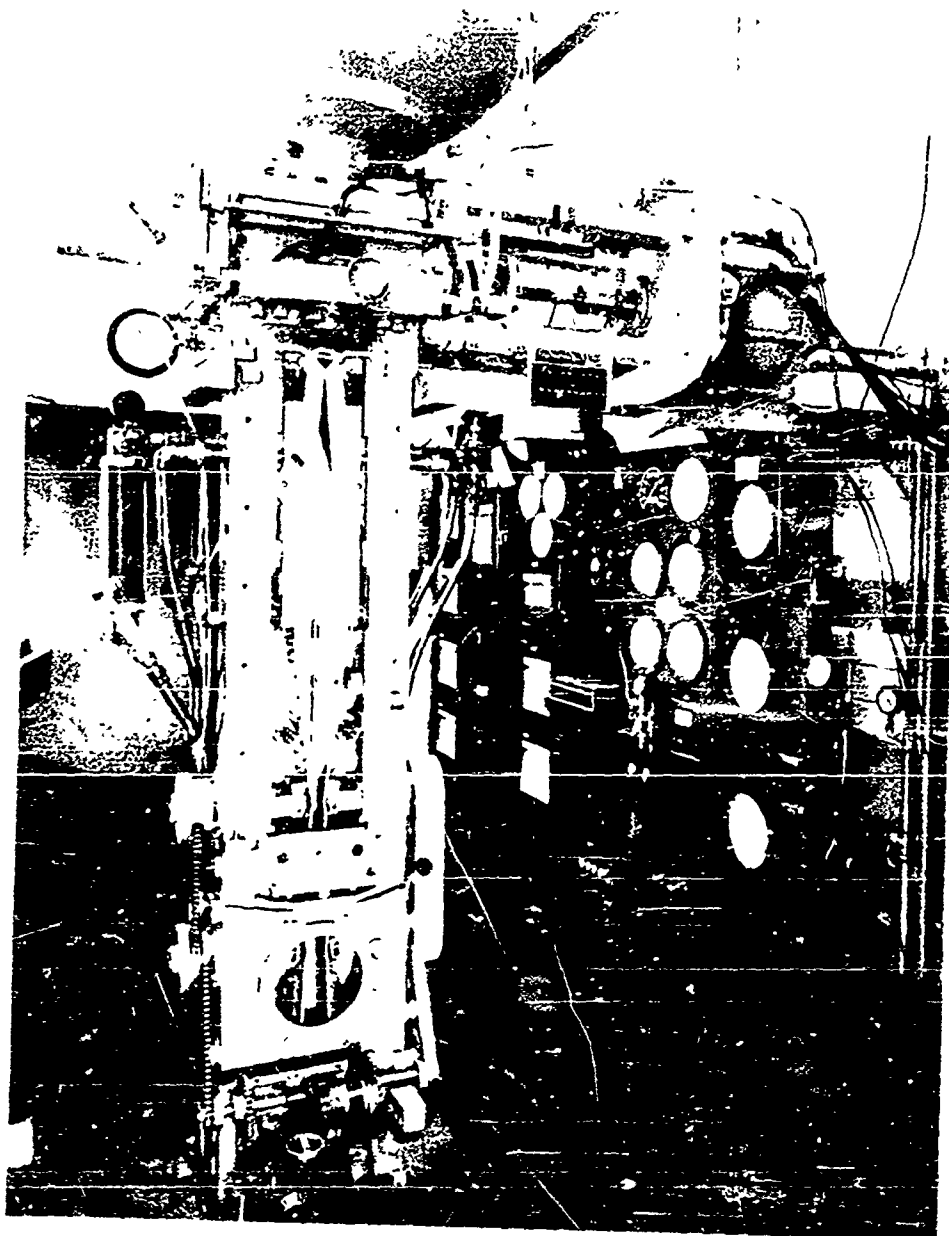
FIG.1 THE NOL 12X12 CM HYPERSONIC TUNNEL NO.4
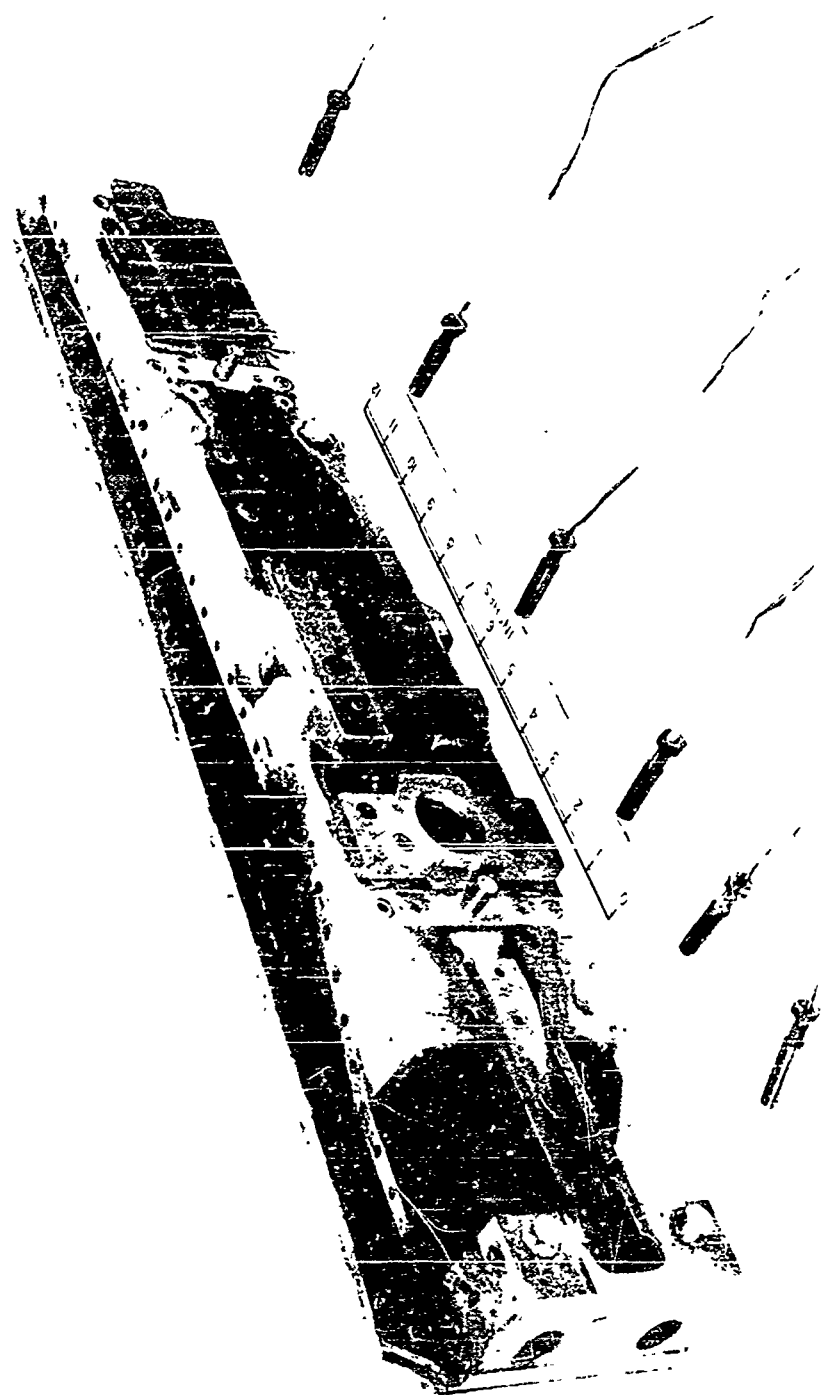
FIG. 2
COOLED WEDGE NOZZLE BLOCK WITH THERMOCOUPLE PLUGS REMOVED

FIG-3
COOLED WEDGE
NOZZLE
FOR
TUNNEL NO.4
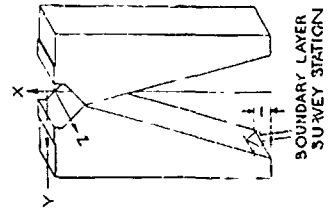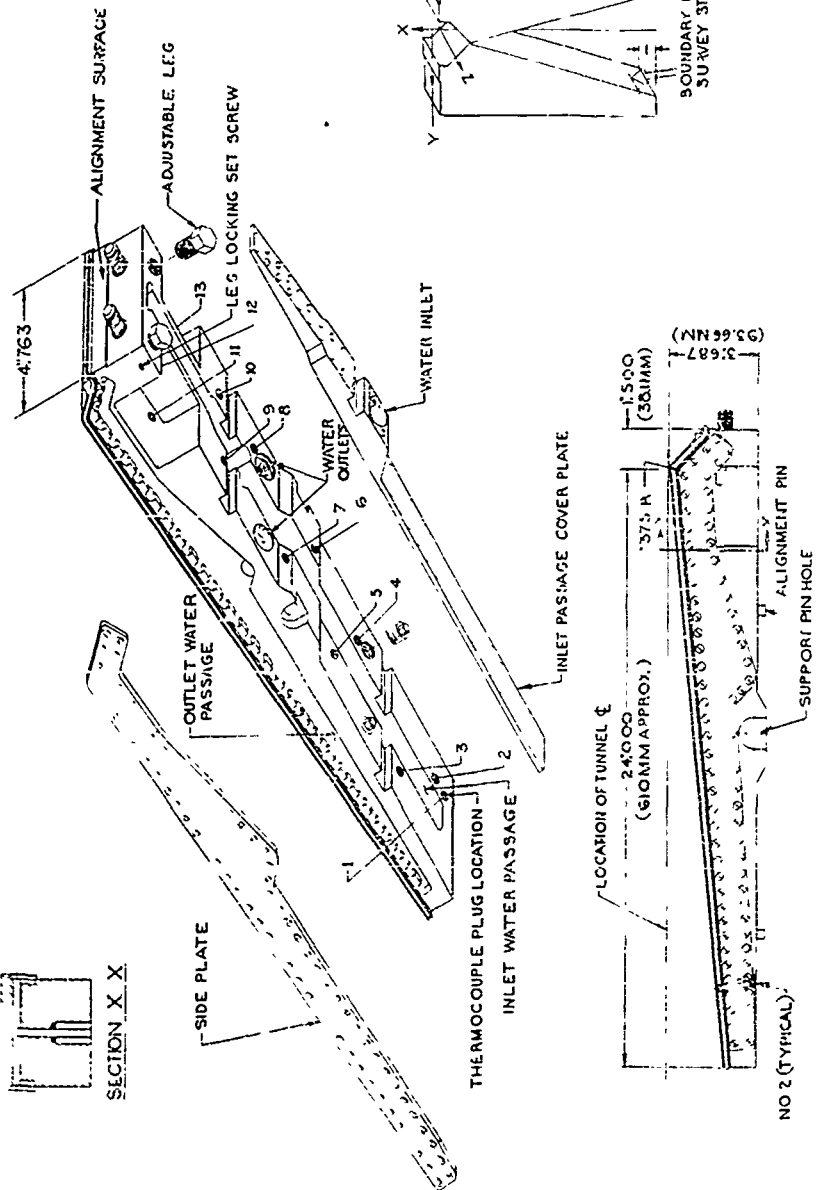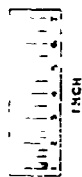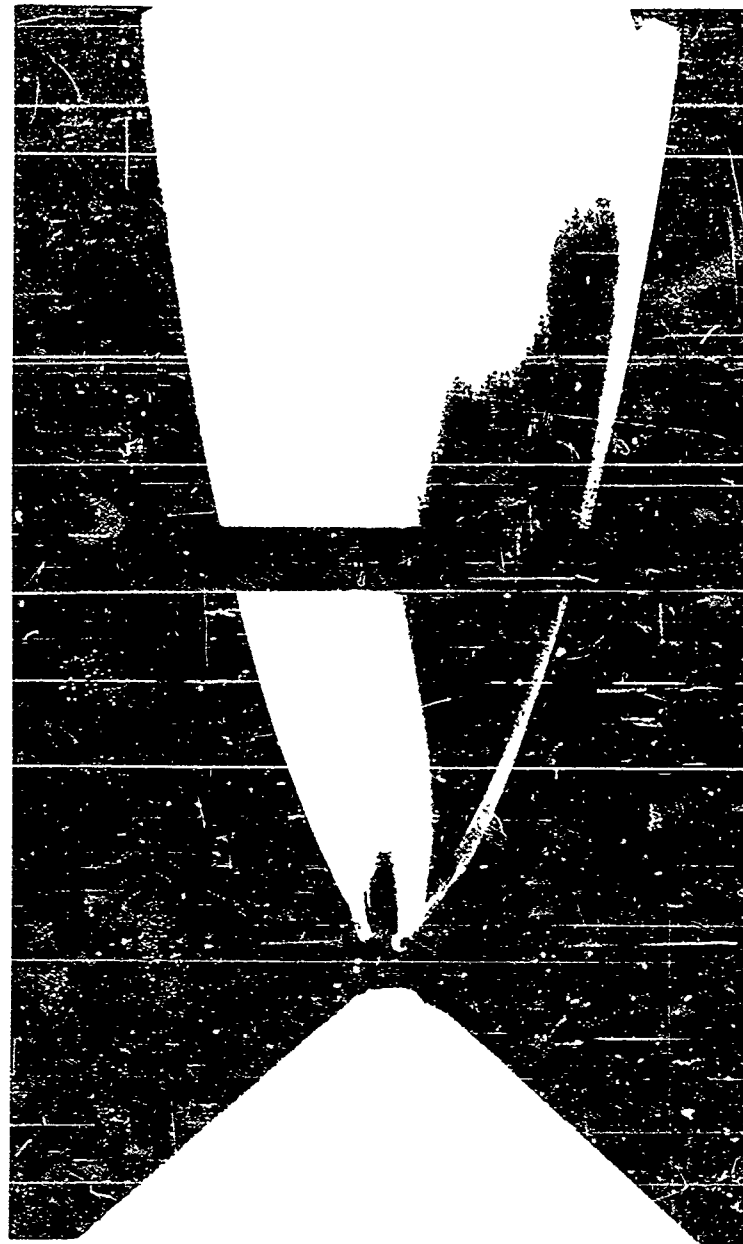
FIG. 4 SCHLIEREN PHOTOGRAPH OF THE FLOW NEAR THE THROAT OF A MINIMUM LENGTH: M = 5.18, NOZZLE: $T_0 = 333\ °K$ $P_0 = 4.5$ atm

(SHADOWGRAPH)

FLOW DIRECTION →
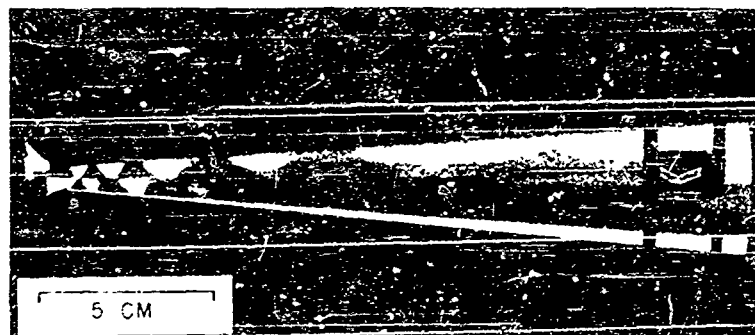
(SCHLIEREN)

(a) THROAT REGION, $M_S = 5.0$, $P_0 = 4$ atm, $T_0 = 293°K$
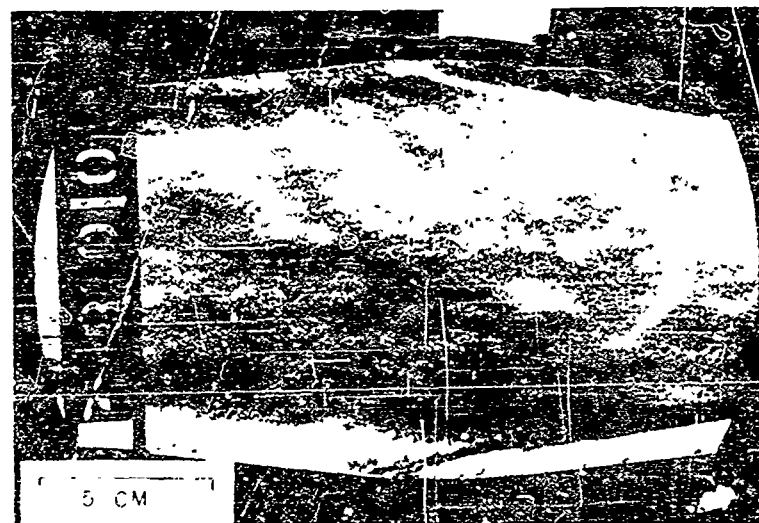
(SCHLIEREN)

(b) NOZZLE EXIT, $M = 70$, $P_0 = 20$ atm, $T_0 = 293°K$

FIG. 5 SHADOWGRAPH AND SCHLIEREN PHOTOGRAPHS
OF FLOW IN THE WEDGE NOZZLE
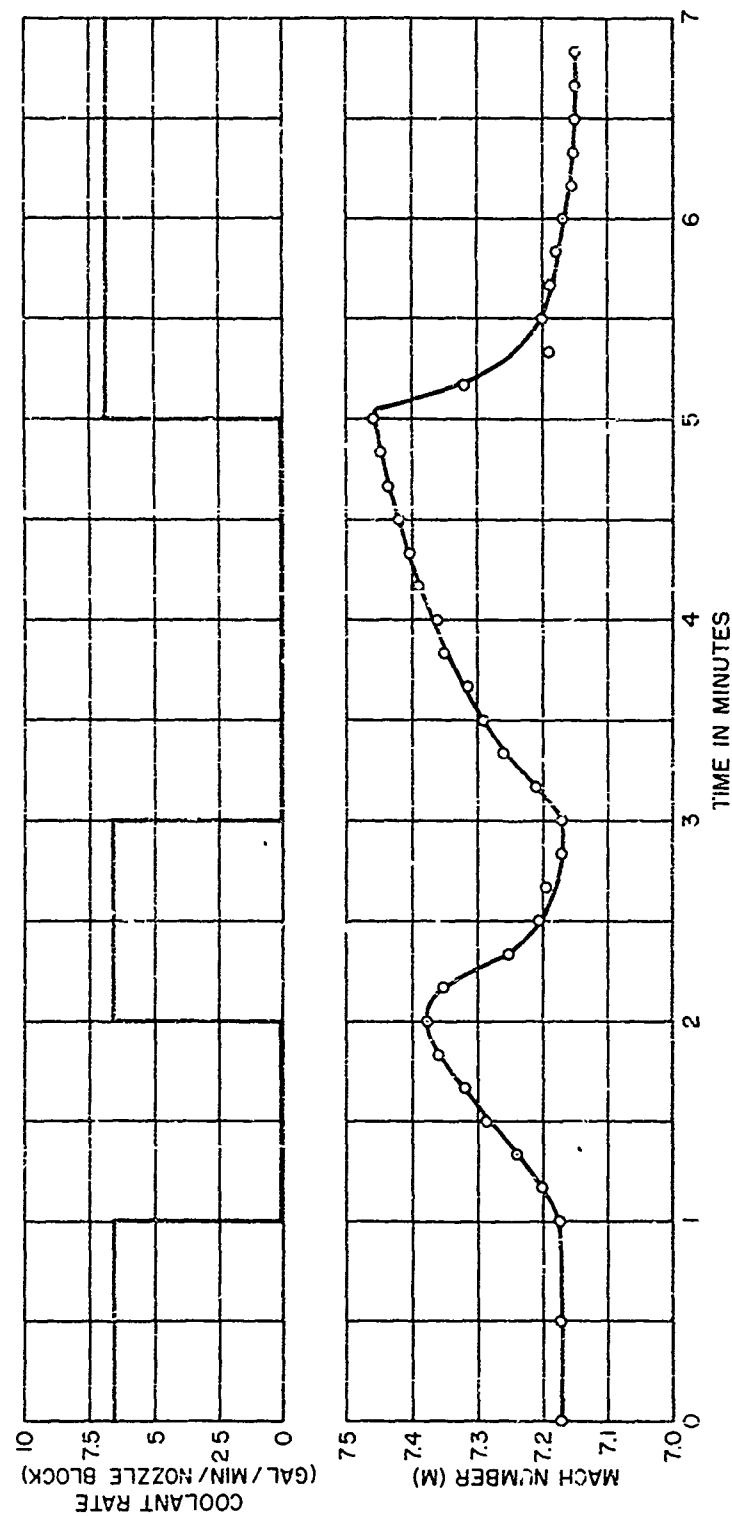
FIG. 6 MACH NUMBER VARIATION IN NOZZLE EXIT vs TIME
FOR CHANGING COOLANT RATE
$P_0 = 10\ atm,\ T_0 = 593°\,F$
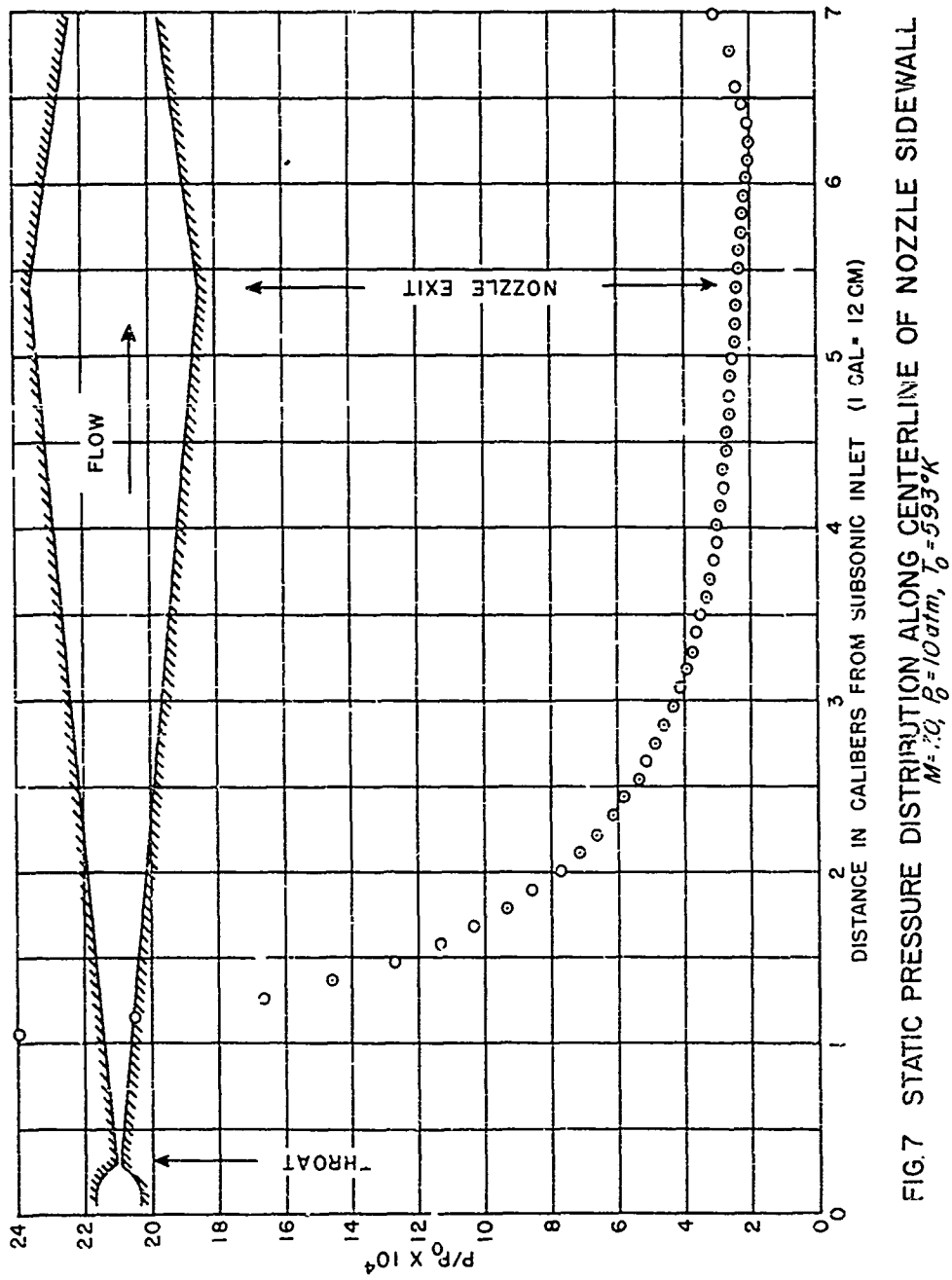
FIG.7 STATIC PRESSURE DISTRIBUTION ALONG CENTERLINE OF NOZZLE SIDEWALL
$M=2.0$, $P_0=10 atm$, $T_0=593°K$
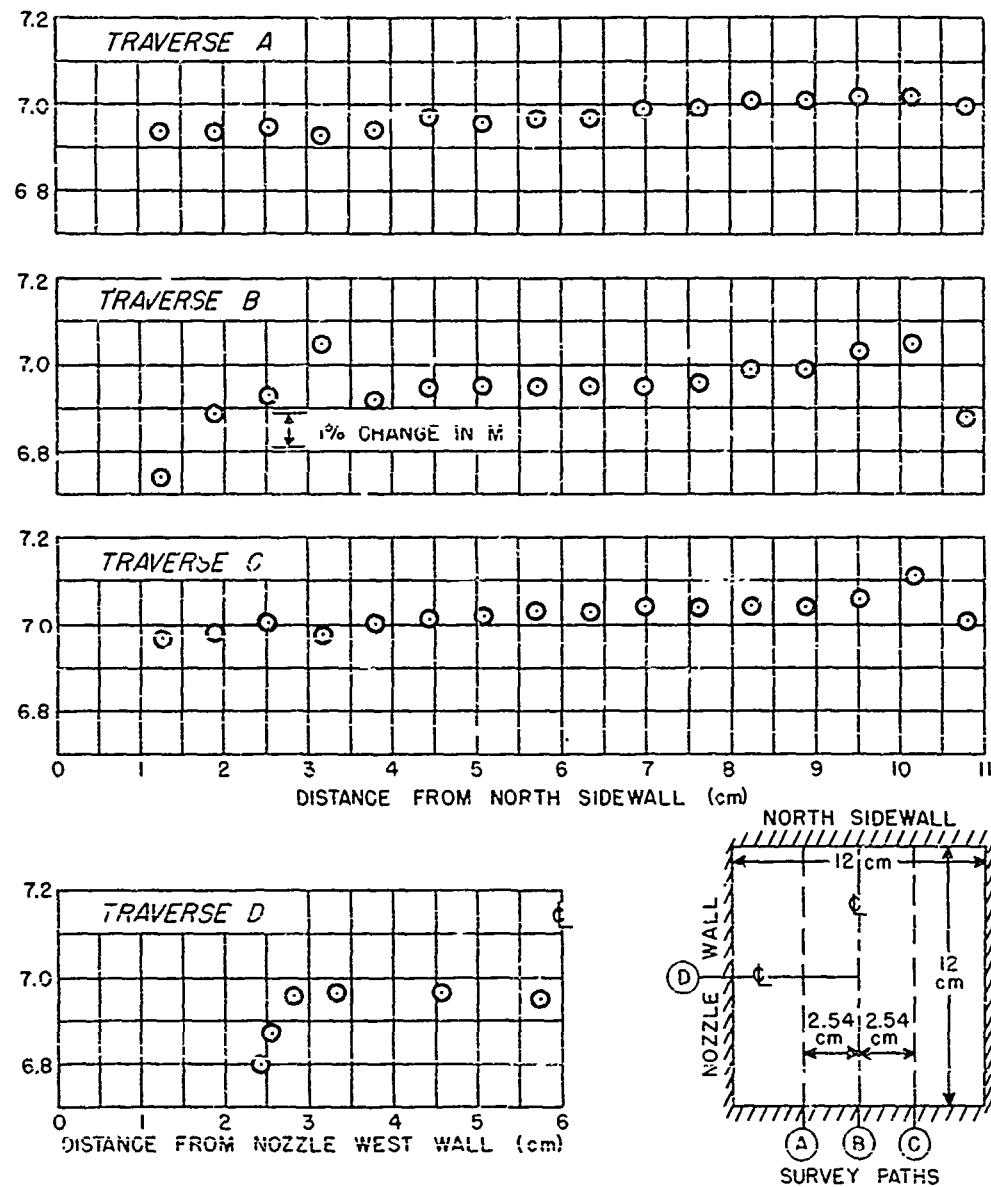
FIG. 8. MACH NUMBER DISTRIBUTIONS ALONG SURVEYS IN A PLANE
ONE INCH UPSTREAM FROM THE NOZZLE EXIT
$P_0 = 10$ atm, $T_0 = 593°K$
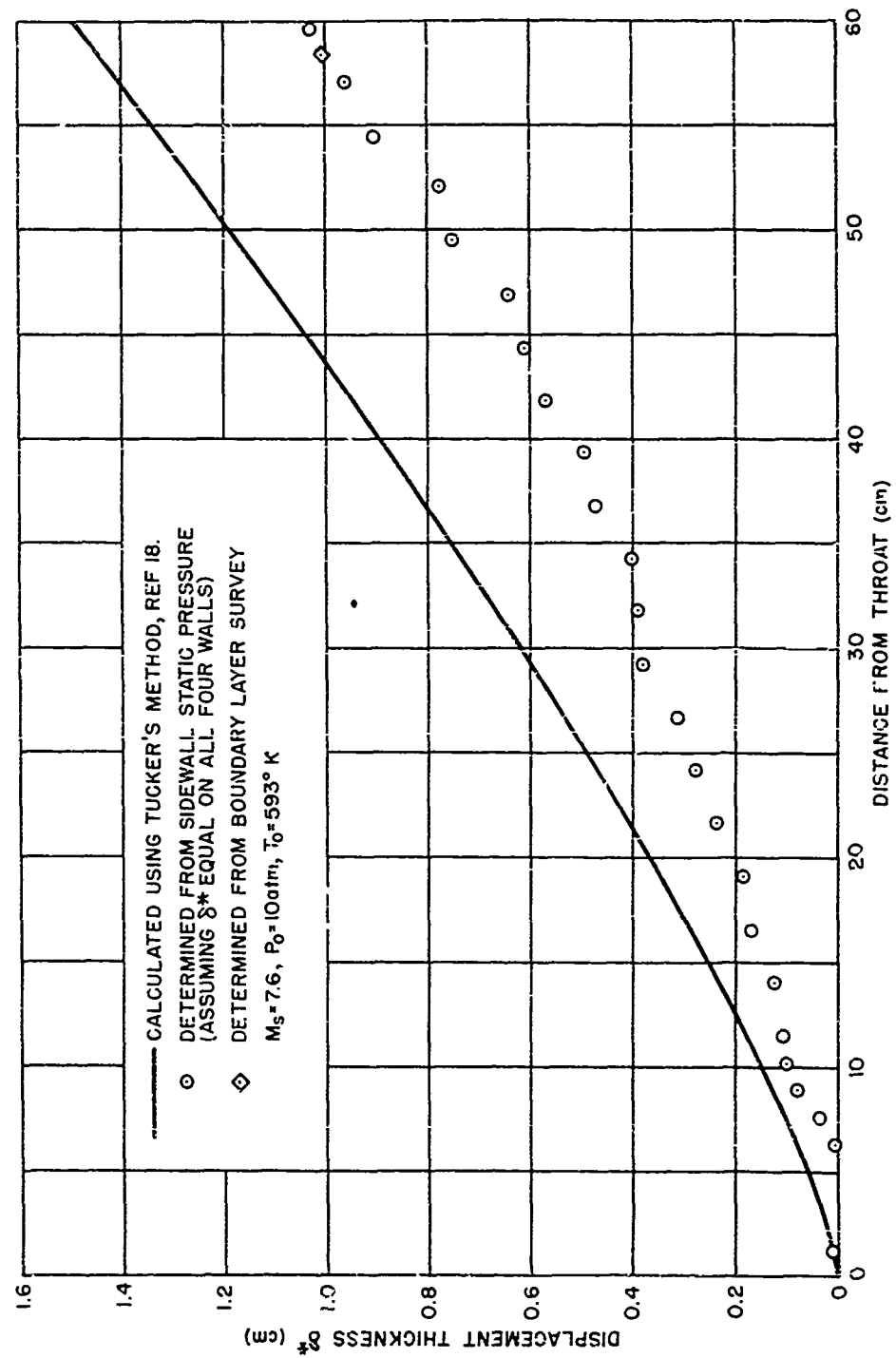
FIG. 9 COMPARISON OF MEASURED AND CALCULATED
BOUNDARY LAYER GROWTH ALONG NOZZLE WALL
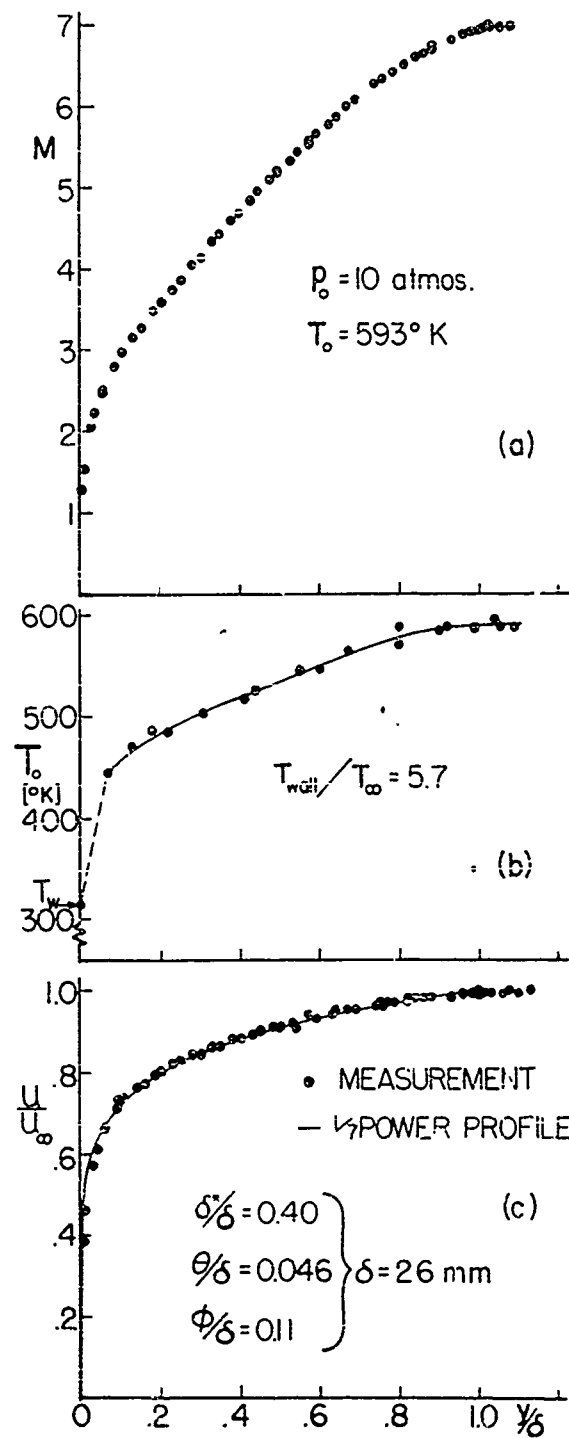
FIG. 10 MEASURED TURBULENT BOUNDARY LAYER PROFILES
WITH HEAT TRANSFER AT A FREE STREAM MACH NUMBER OF 7
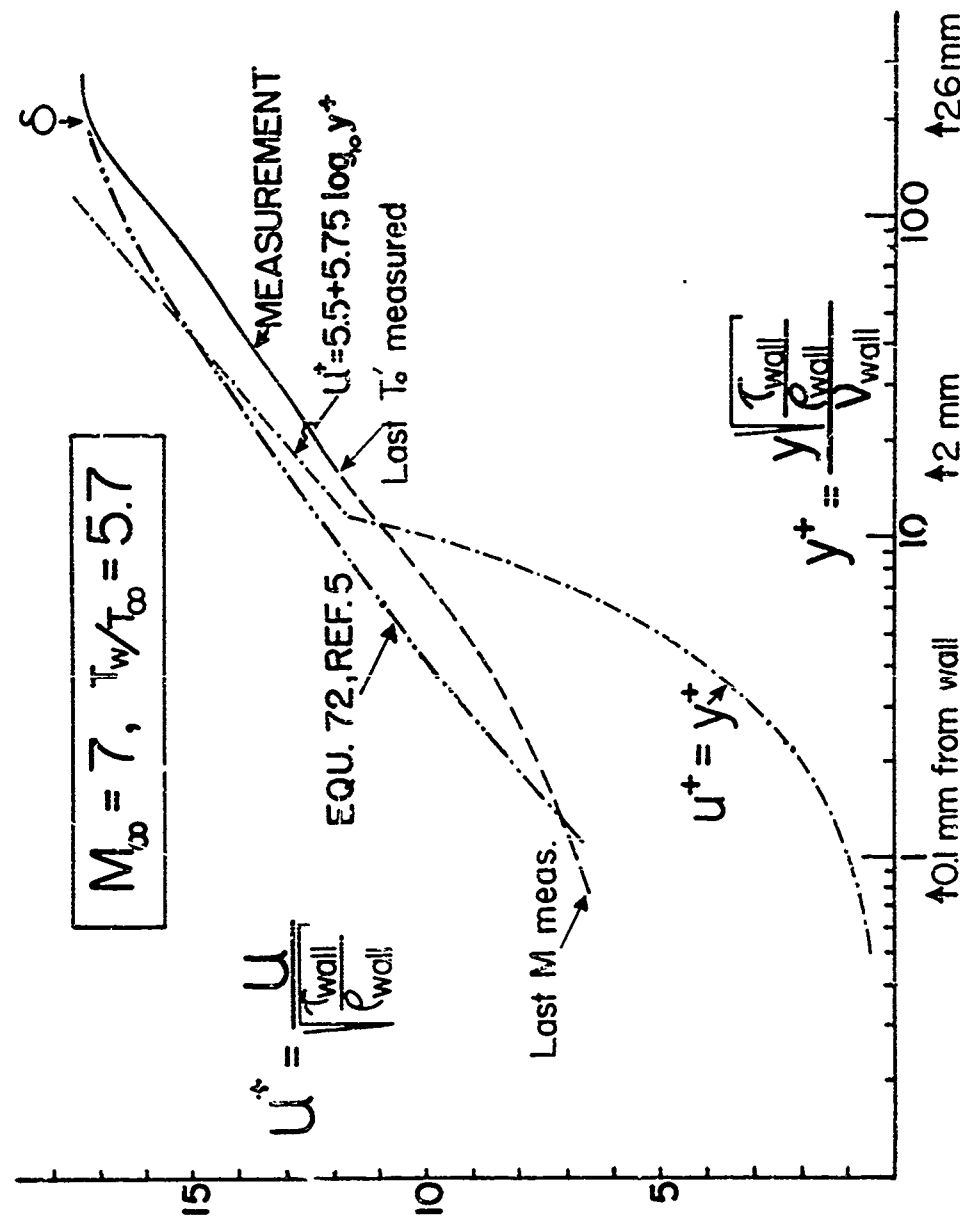
FIG. II THE u^+, y^+ REPRESENTATION OF THE MEASURED VELOCITY PROFILES AT $M_1 = 7$ AND COMPARISON WITH THEORY
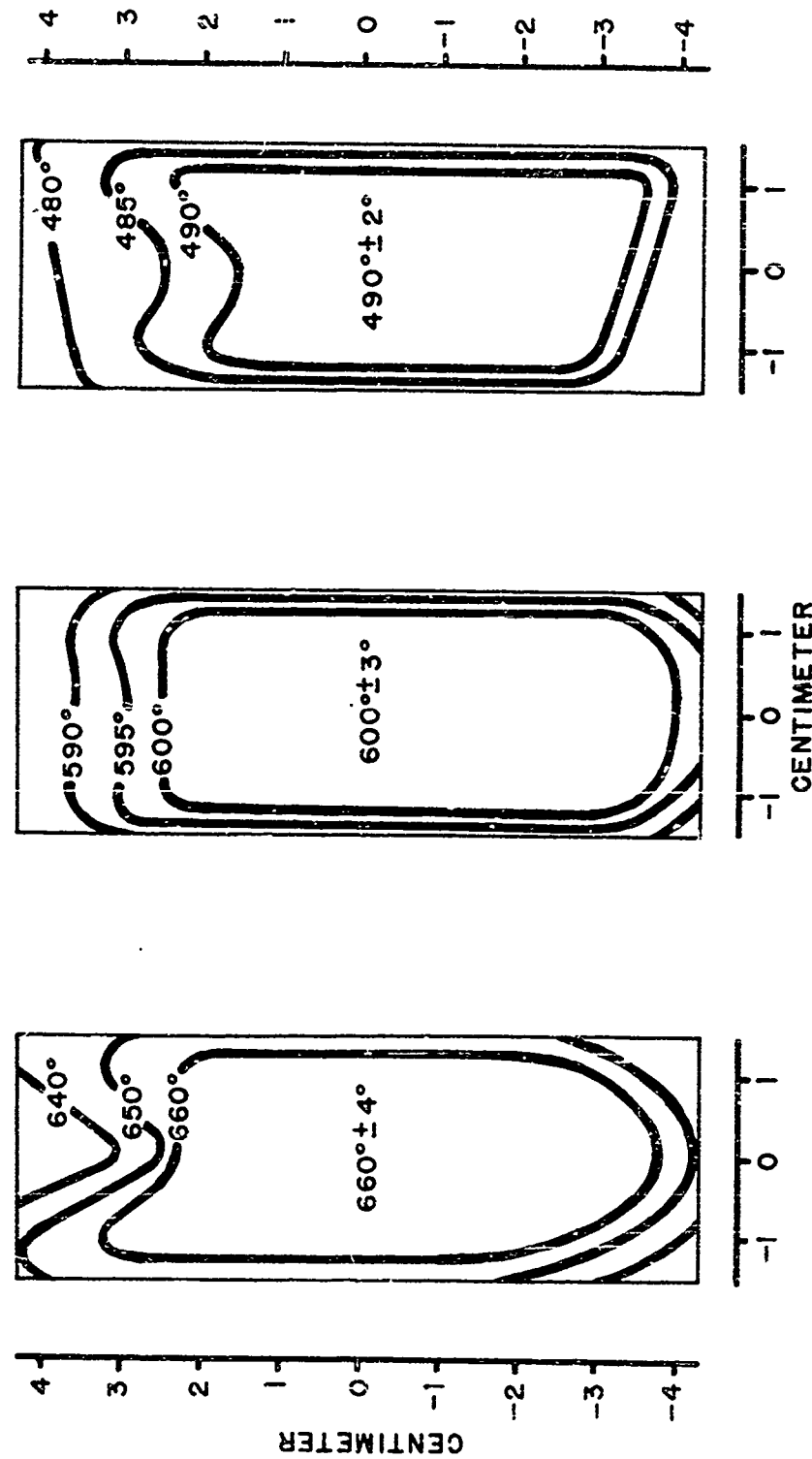
FIG. 12   TEMPERATURE DISTRIBUTION IN NOZZLE INLET
AT THREE DIFFERENT LEVELS OF SUPPLY TEMPERATURE
(TEMPERATURES IN °K)
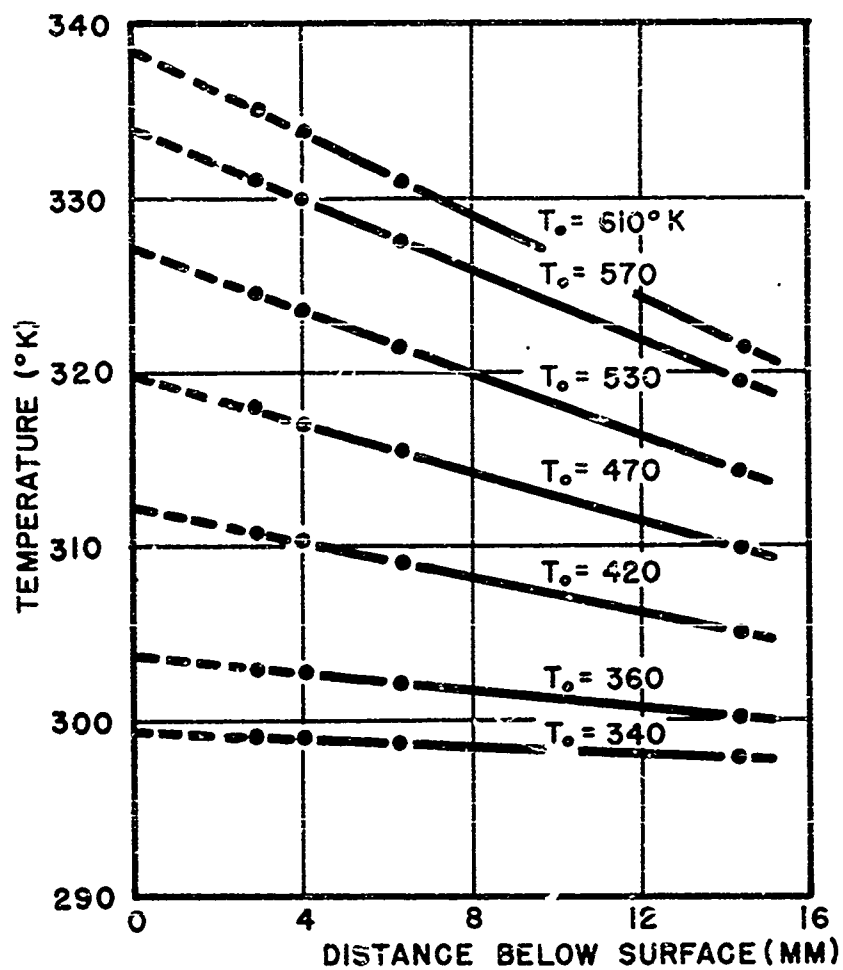
FIG. 13 NOZZLE WALL-TEMPERATURES NEAR THROAT
(STATION NO. 13) AT VARIOUS SUPPLY TEMPERATURES

$P_o = 10$ ATM , $M_S = 7.6$
COOLING RATE: 6.5 GALLONS/MIN
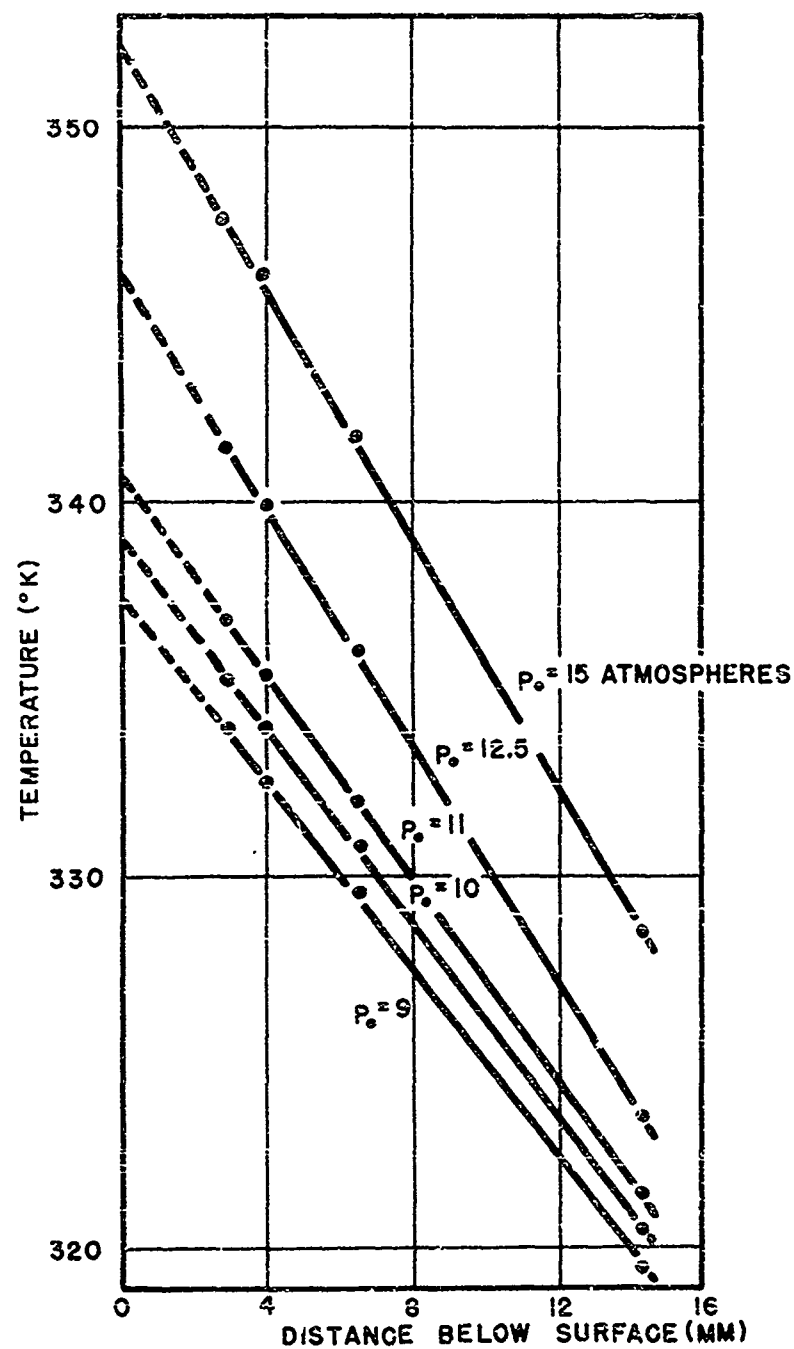
FIG. 14   NOZZLE WALL-TEMPERATURES NEAR THROAT
(STATION NO.13) AT VARIOUS SUPPLY PRESSURES
$T_o = 610° K$, $M_S = 7.6$
COOLING RATE: 6.5 GALLONS / MIN
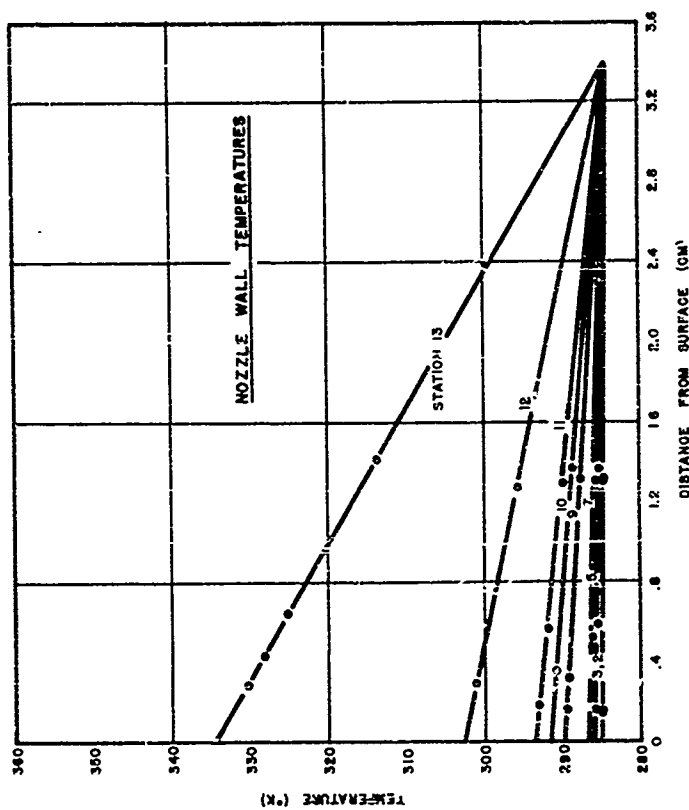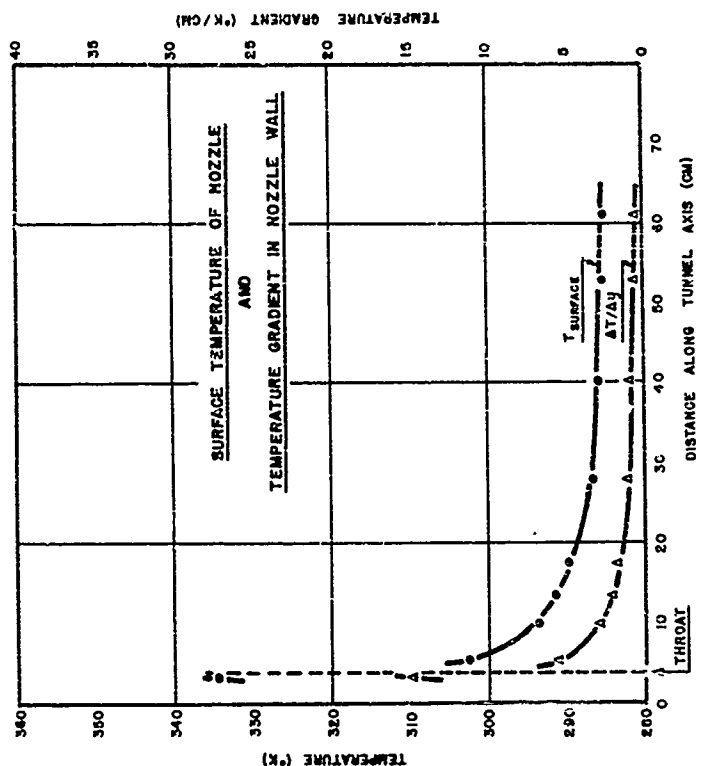
FIG. 15 WALL TEMPERATURES AT 9 STATIONS, TEMPERATURE GRADIENT IN WALL,
AND EXTRAPOLATED SURFACE TEMPERATURES OF NOZZLE

$M_S = 7.6$ $P_o = 10$ ATM $T_o = 593°K$
COOLING RATE: 6.5 GALLONS PER MINUTE
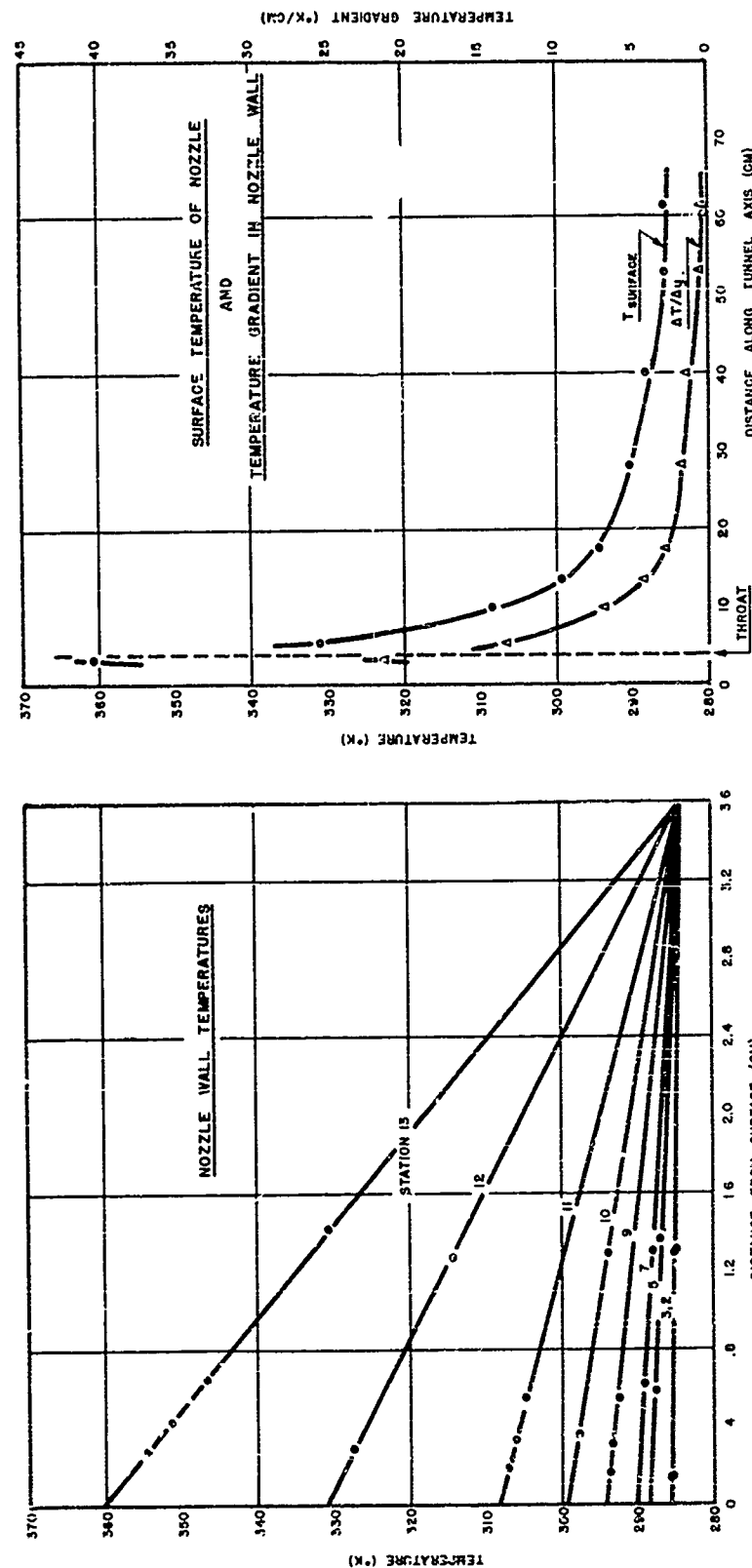
FIG. 16 WALL TEMPERATURES AT 9 STATIONS, TEMPERATURE GRADIENT IN WALL, AND EXTRAPOLATED SURFACE TEMPERATURES OF NOZZLE
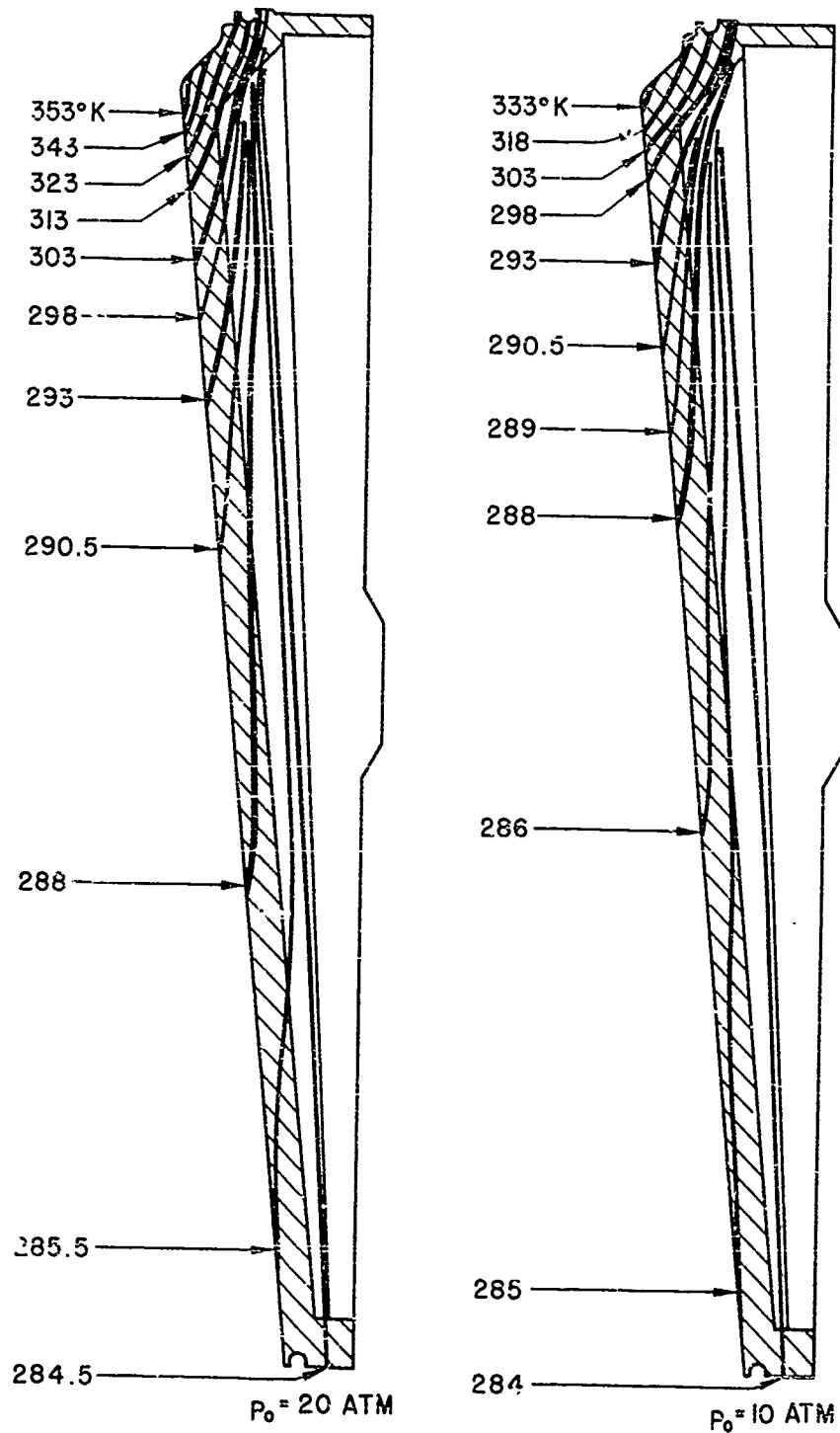
FIG. 17 ISOTHERMS IN NOZZLE
FOR
$M_3 = 7.6$ $T_0 = 593°K$ $P_0 = 10$ AND 20 ATM
COOLING RATE: 6.5 GALLONS PER MINUTE
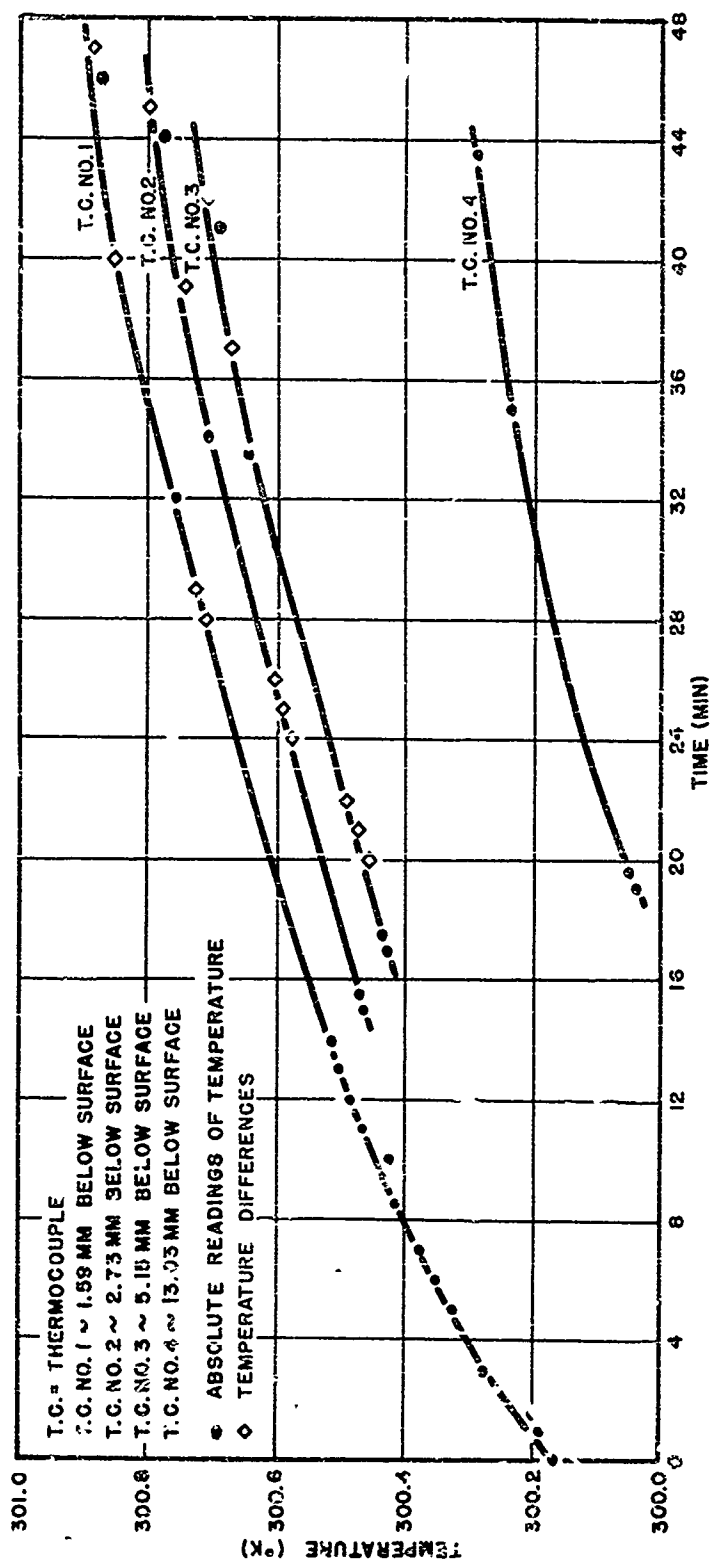
FIG. 18 NOZZLE WALL-TEMPERATURES AS FUNCTION OF RUNNING TIME
AT BOUNDARY LAYER SURVEY STATION

$M_S = 7.6$, $P_o = 21.4$ ATM, $T_o = 593°K$
COOLING RATE: 6.5 GALLONS/MIN

$$\frac{\Delta T}{\Delta y} = .048 \frac{°K}{MM}$$
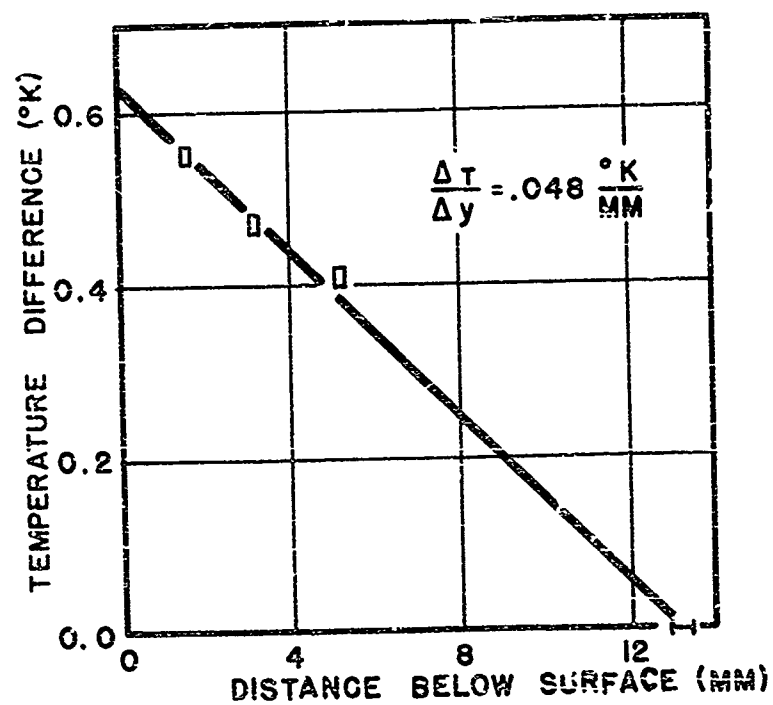
ERROR $\begin{cases} \text{DISTANCE: } \pm 0.1 \text{ MM} \\ \Delta T: \pm 0.01°K \end{cases}$

FIG. 19 TEMPERATURE DROP IN NOZZLE WALL

$M_S = 7.6$, $P_o = 21.4$ ATM, $T_o = 593°K$
COOLING RATE: 5.5 GALLONS/MIN
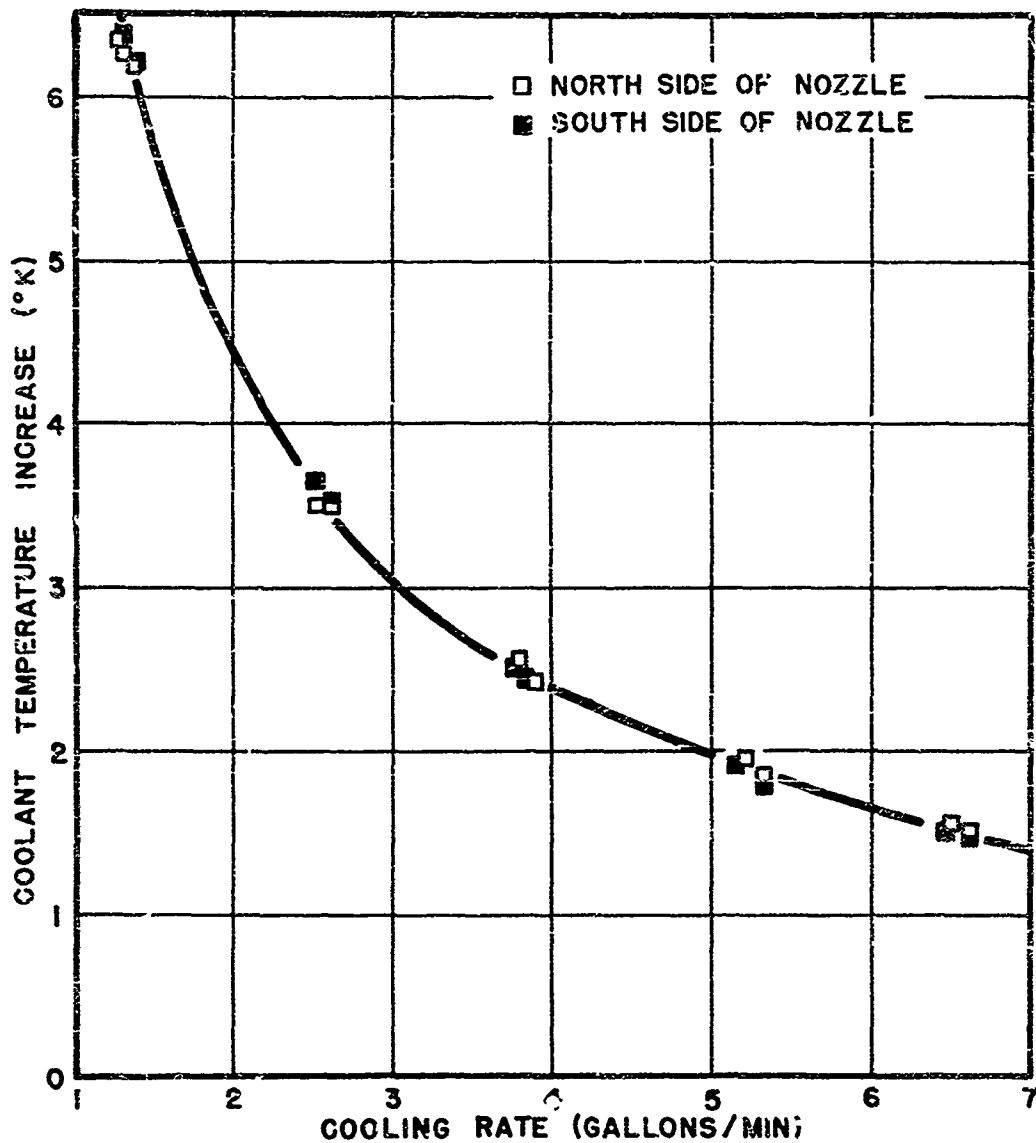
FIG. 20 TEMPERATURE INCREASE OF COOLING WATER
AS FUNCTION OF THE COOLING RATE FOR
TUNNEL OPERATION

$M_S = 8.0$, $P_o = 20$ ATM, $T_o = 800°K$
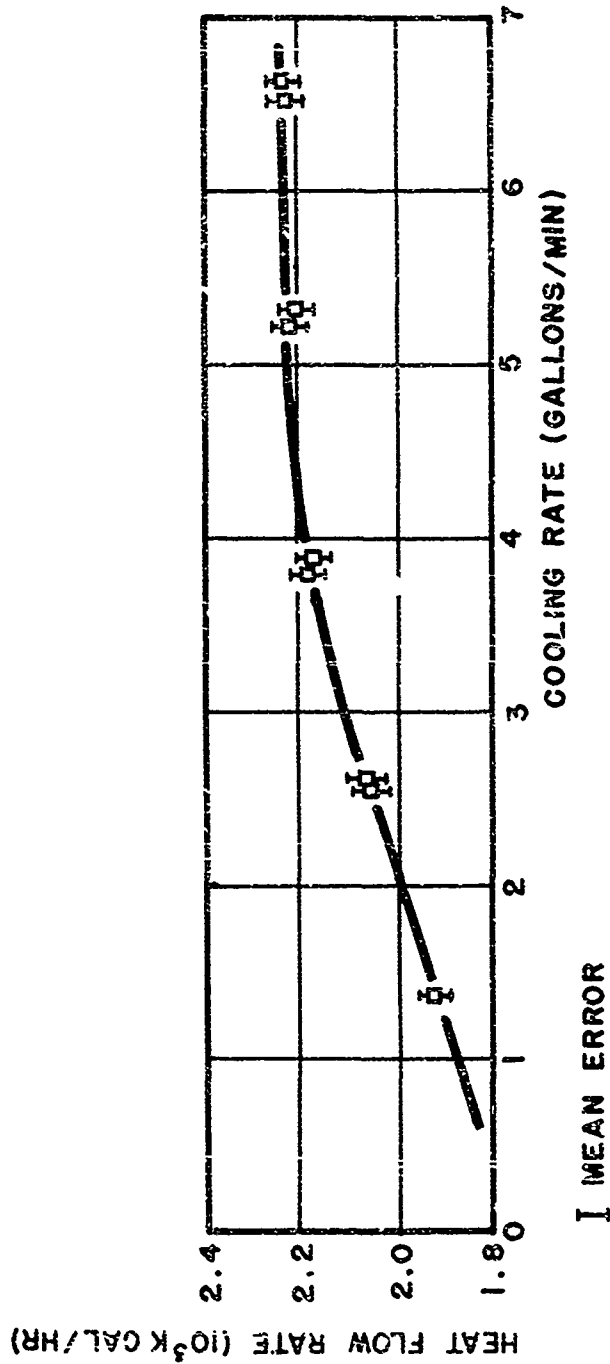
FIG. 21 HEAT FLOW RATE TO COOLING WATER AS FUNCTION
OF COOLING RATE FOR TUNNEL OPERATION

$M_S = 8.0$, $P_o = 20$ATM, $T_o = 600°$K
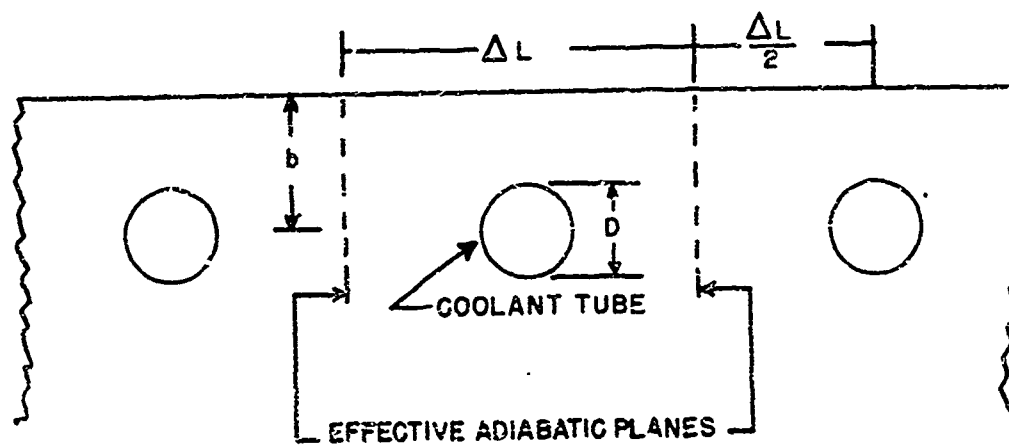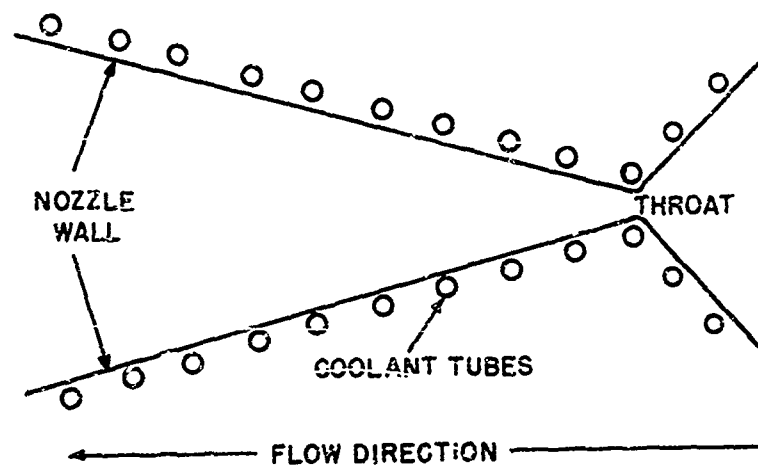
FIG. 22 COOLANT TUBE POSITIONS AND DIMENSIONS
USED IN HEAT TRANSFER ANALYSIS
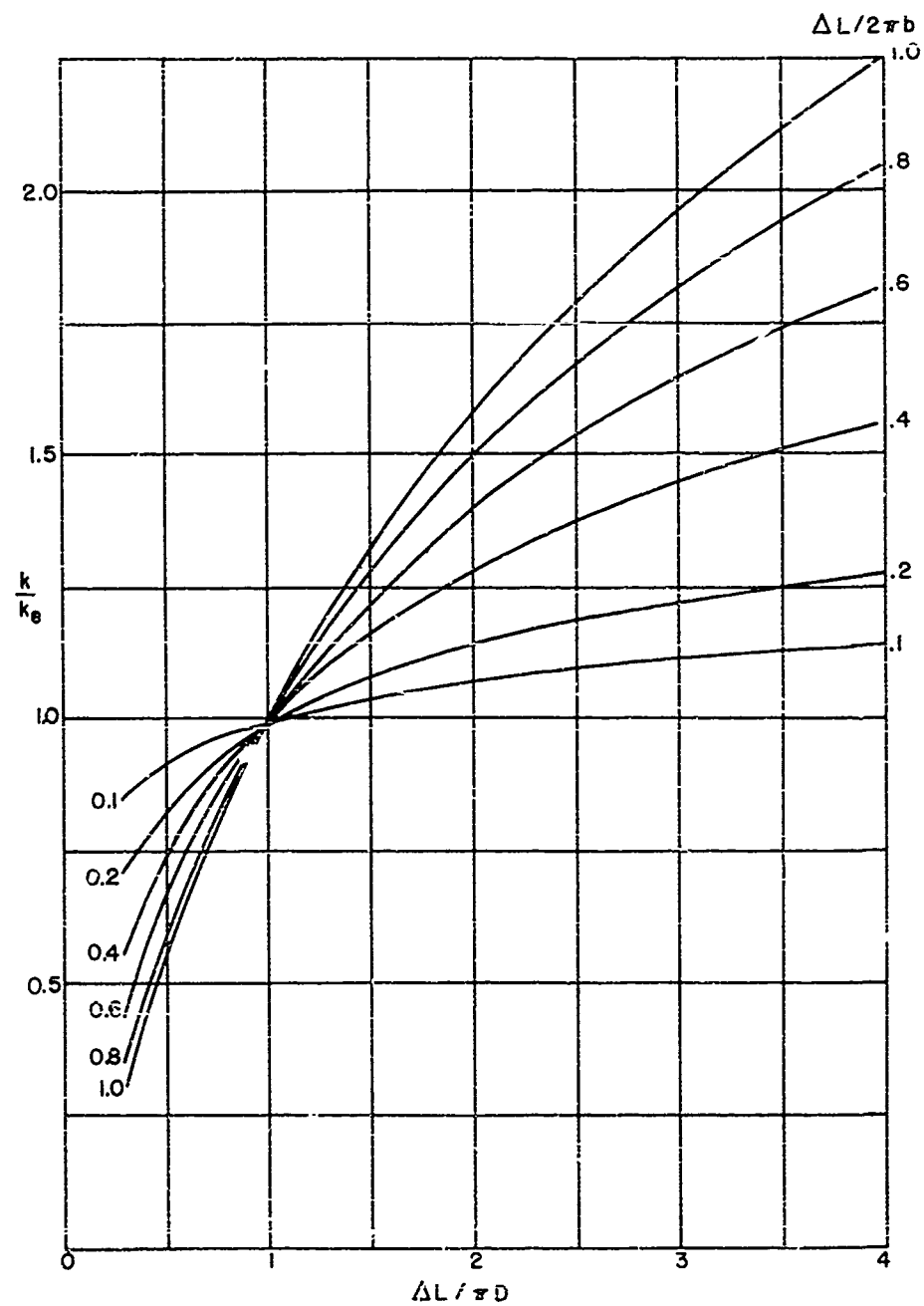
FIG. 23 VARIATION OF k/k_e WITH COOLANT TUBE SIZE AND POSITION
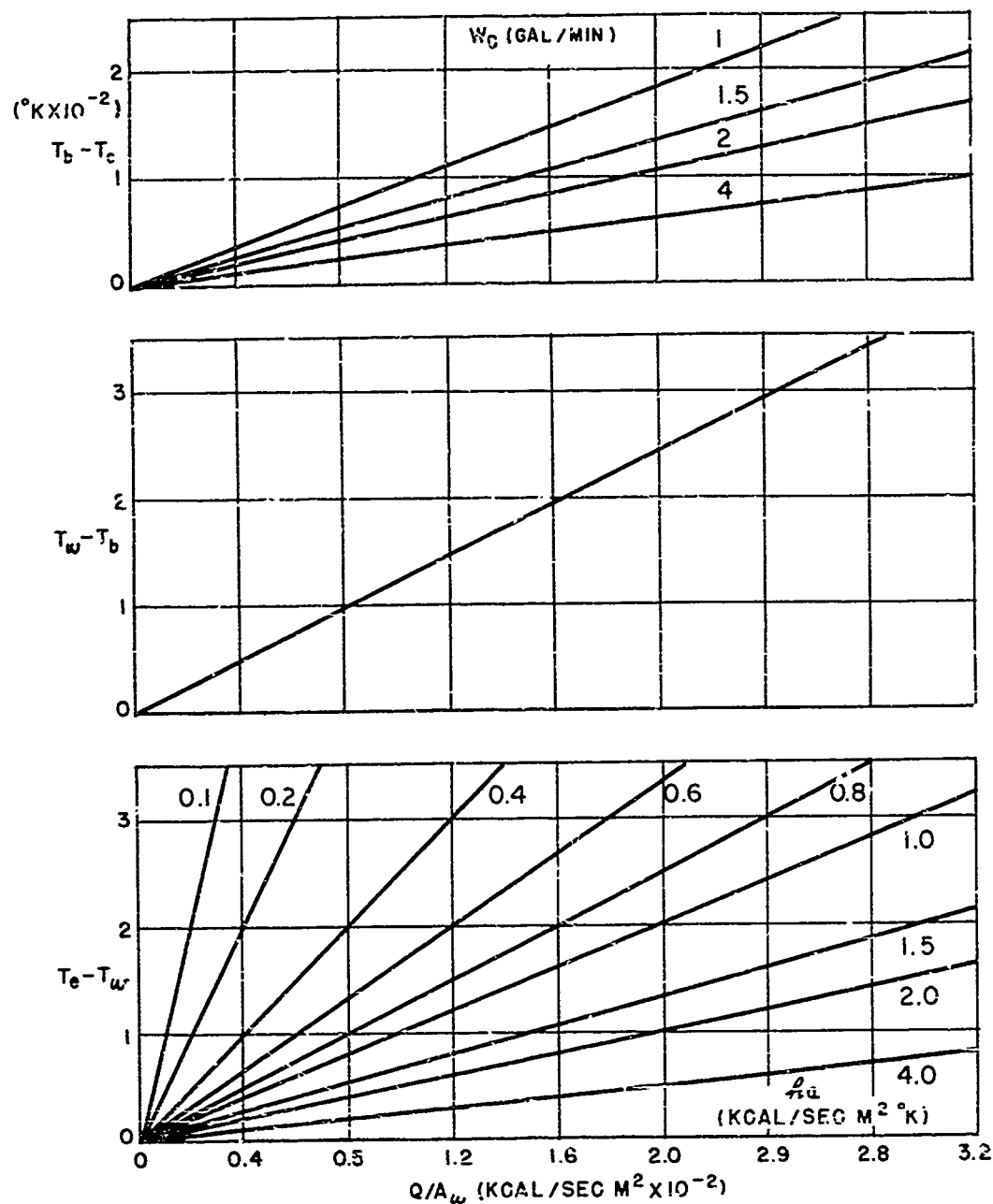
FIG. 24
DETERMINING NOZZLE SURFACE AND COOLANT TUBE SURFACE
TEMPERATURES
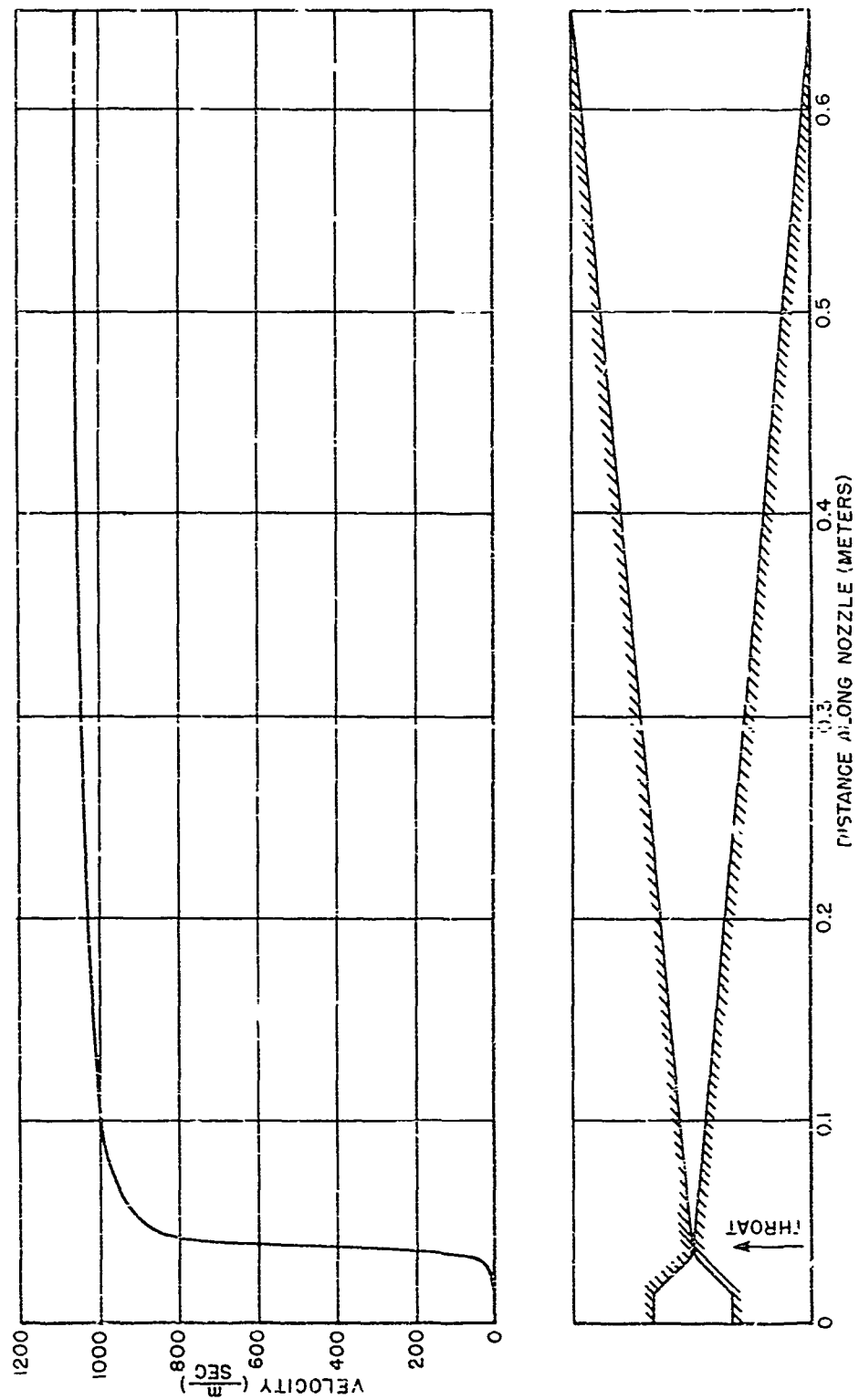
FIG 25 VELOCITY DISTRIBUTION ALONG NOZZLE
$M_s = 8.0, T_0 = 600°K$
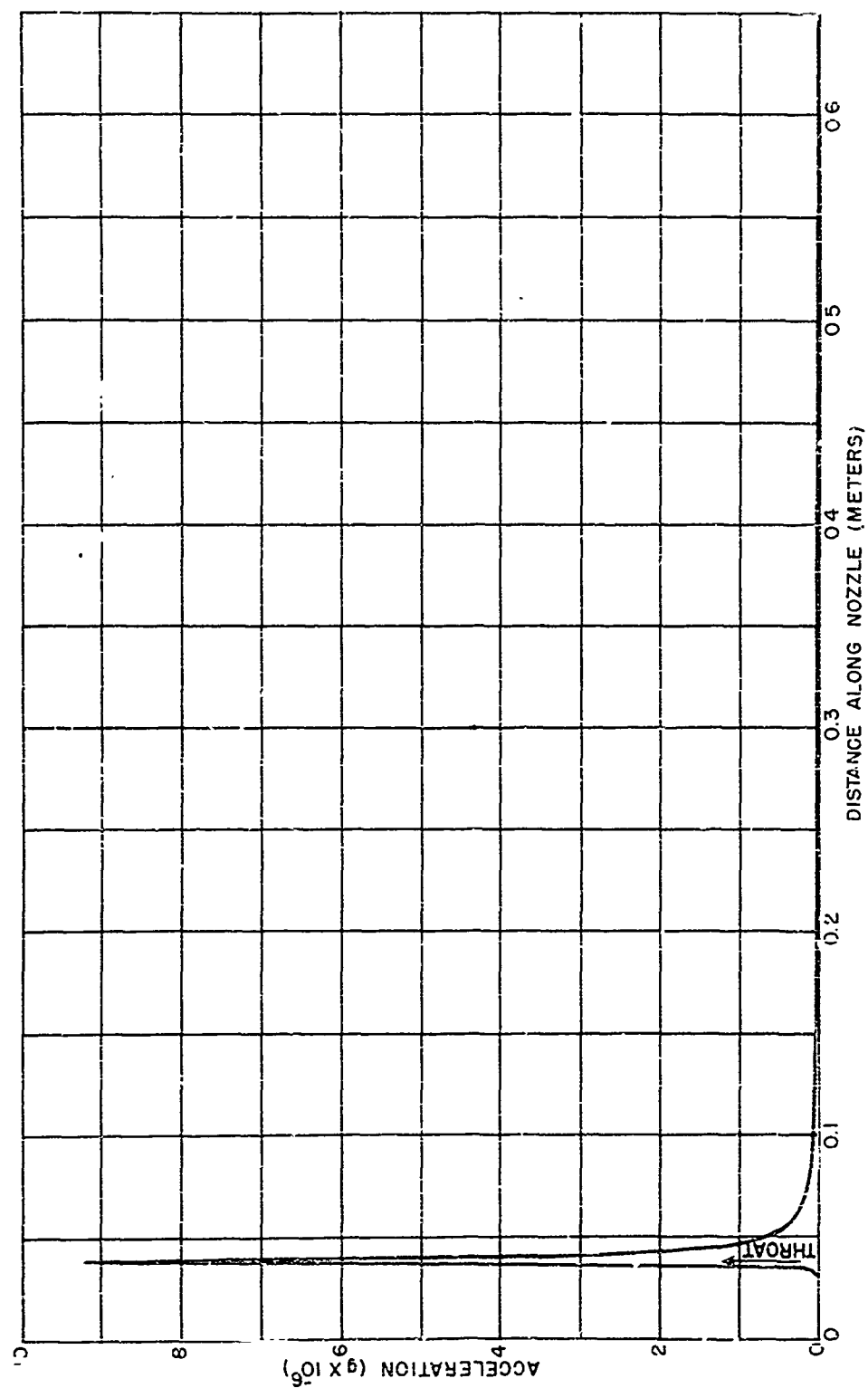
FIG 26 ACCELERATION DISTRIBUTION ALONG NOZZLE
$M_s = 8.0$, $T_0 = 600°K$
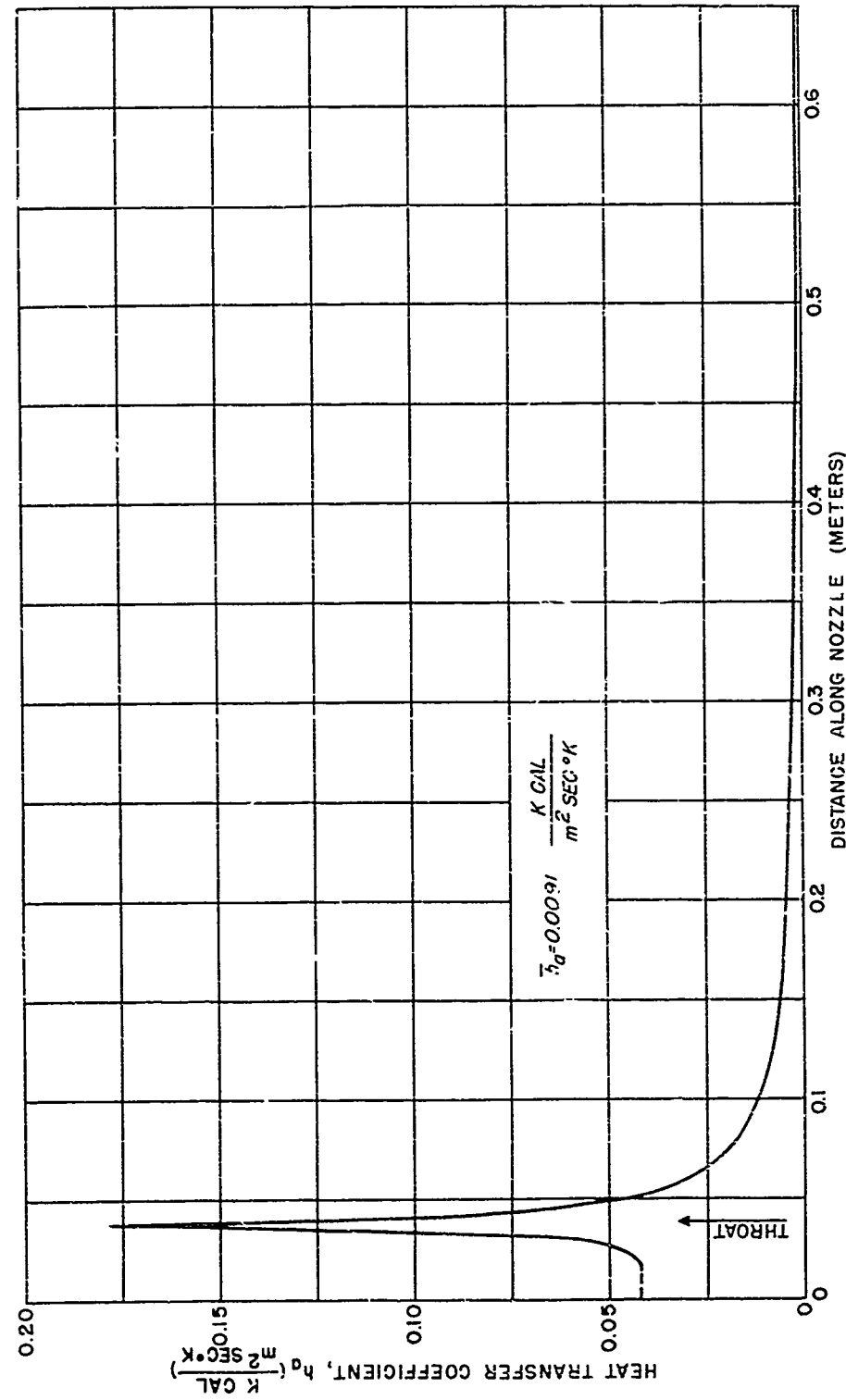
FIG. 27   HEAT TRANSFER COEFFICIENT DISTRIBUTION ASSUMING LAMINAR FLOW
AND NEGLECTING THE EFFECTS OF PRESSURE GRADIENTS
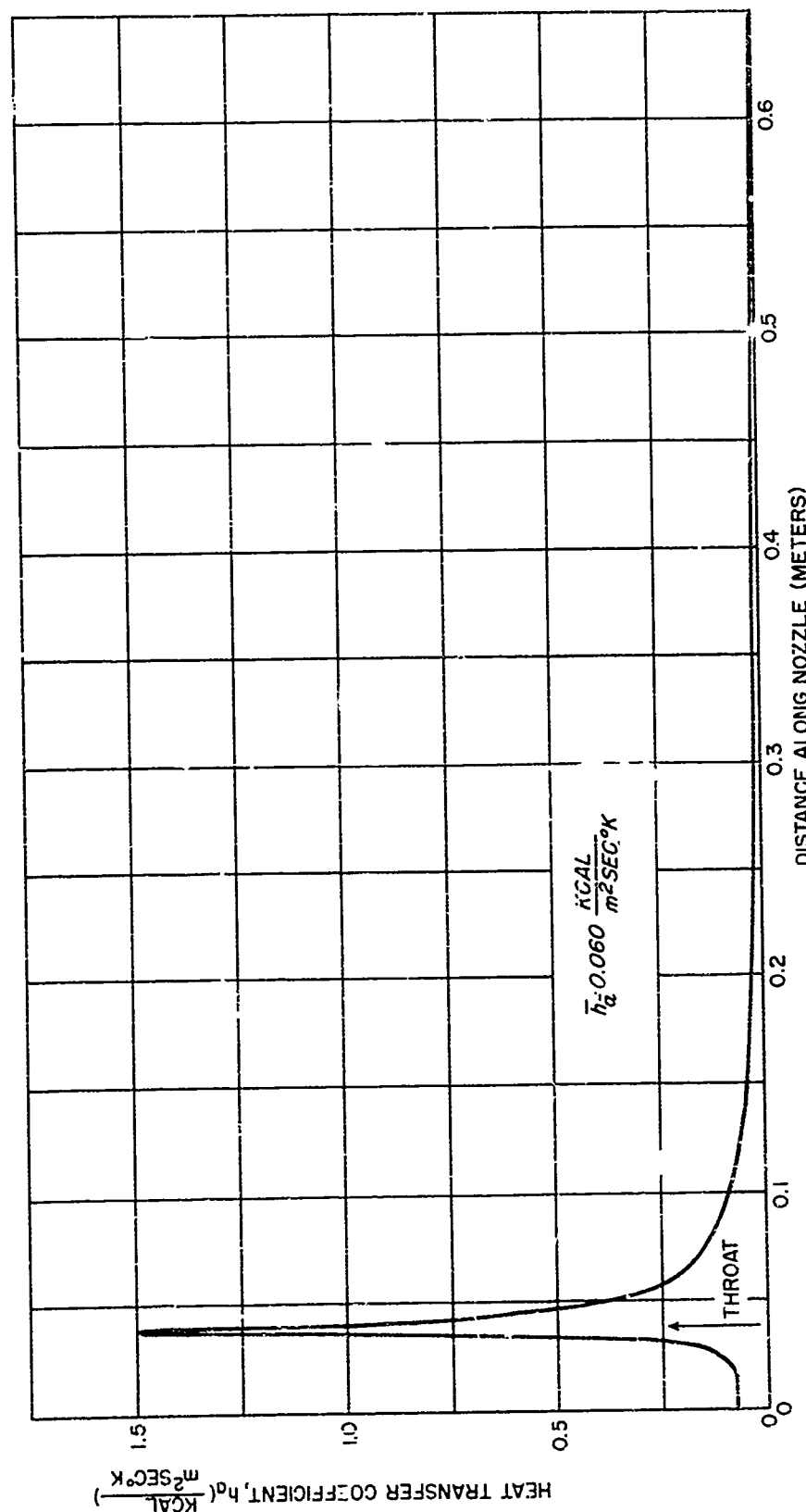$M_s = 8.0, T_0 = 600°K, P_0 = 20 atm$

FIG. 28 HEAT TRANSFER COEFFICIENT DISTRIBUTION ASSUMING TURBULENT FLOW
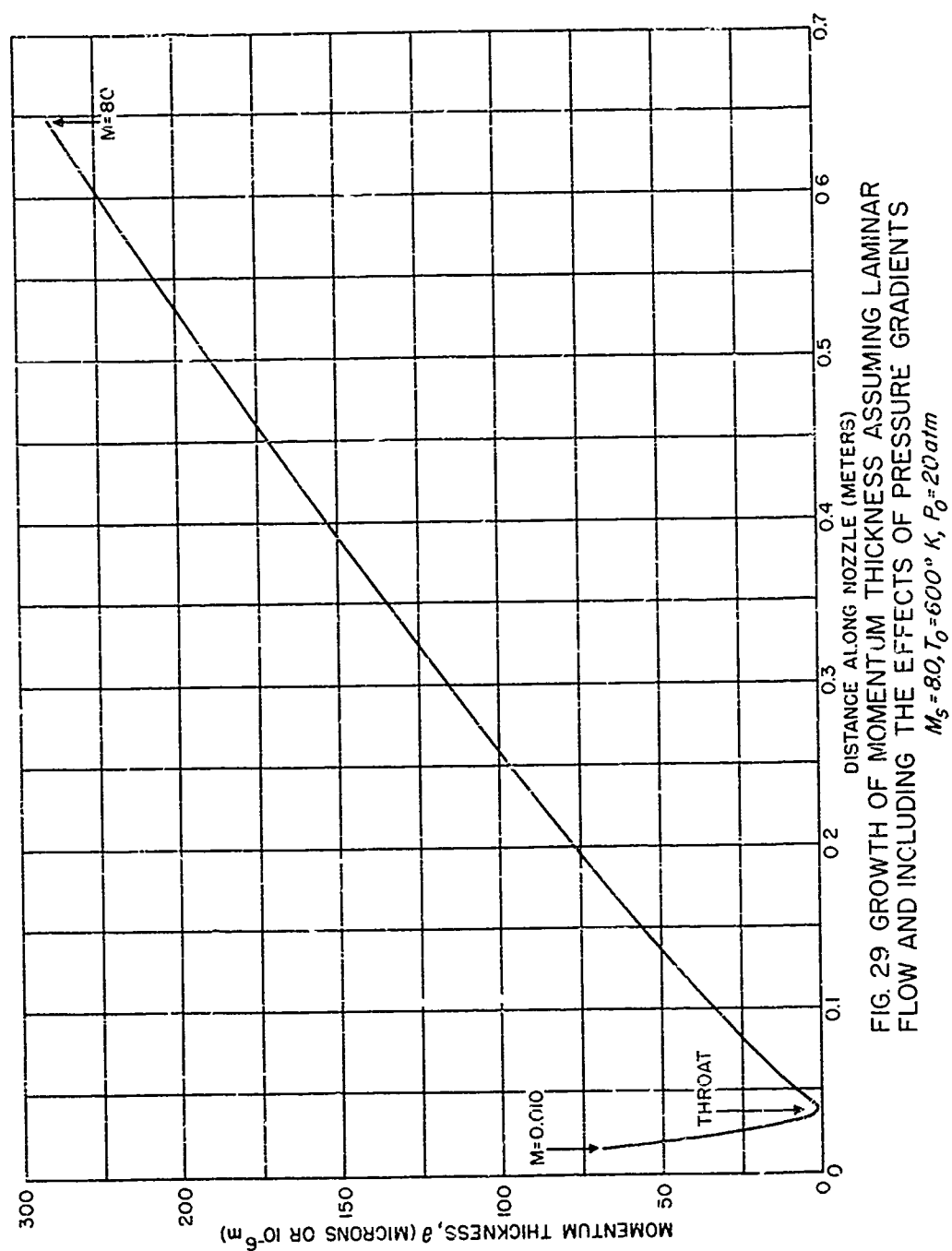AND NEGLECTING THE EFFECTS OF PRESSURE GRADIENTS
$M_s = 8.0, T_0 = 500°K, P_0 = 20 atm$

FIG. 29 GROWTH OF MOMENTUM THICKNESS ASSUMING LAMINAR
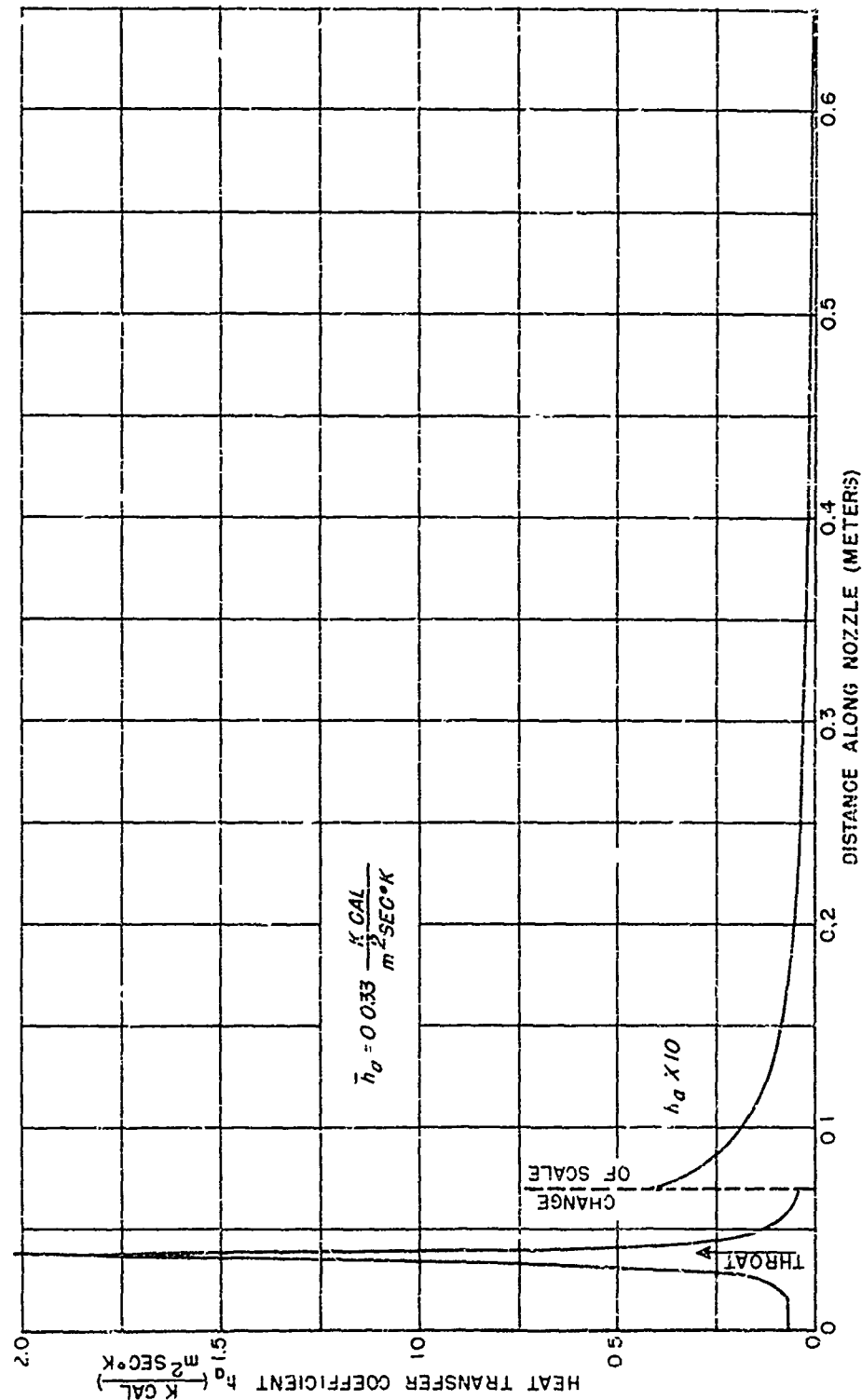FLOW AND INCLUDING THE EFFECTS OF PRESSURE GRADIENTS
$M_s=80, T_0=600°K, P_0=20atm$

FIG. 30 HEAT TRANSFER COEFFICIENT DISTRIBUTION ASSUMING LAMINAR FLOW AND INCLUDING THE EFFECTS OF PRESSURE GRADIENTS
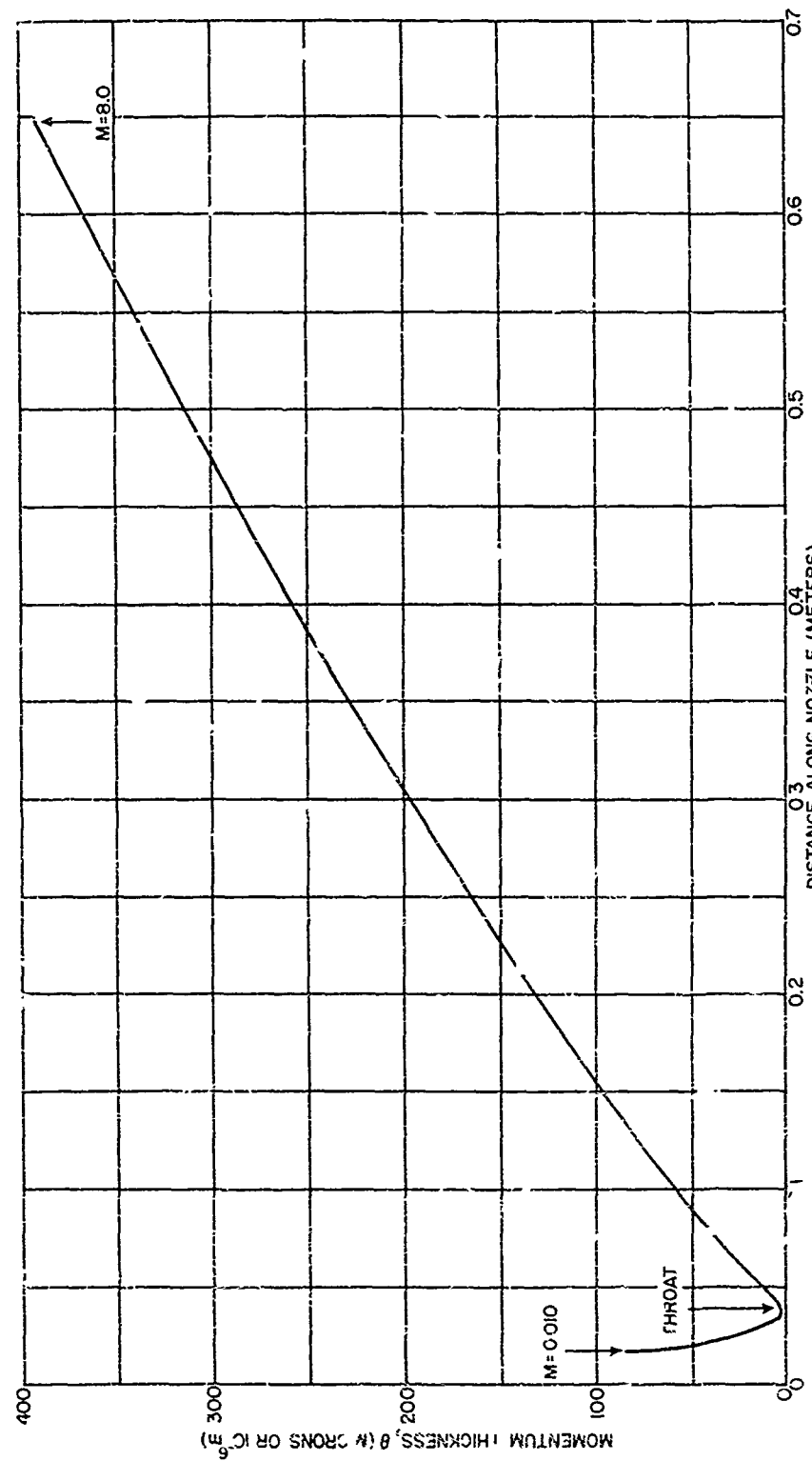
$M_s = 8.0$, $T_0 = 600°K$, $P_0 = 20$ atm

FIG. 31 GROWTH OF MOMENTUM THICKNESS ASSUMING TURBULENT FLOW AND INCLUDING THE EFFECTS OF PRESSURE GRADIENTS
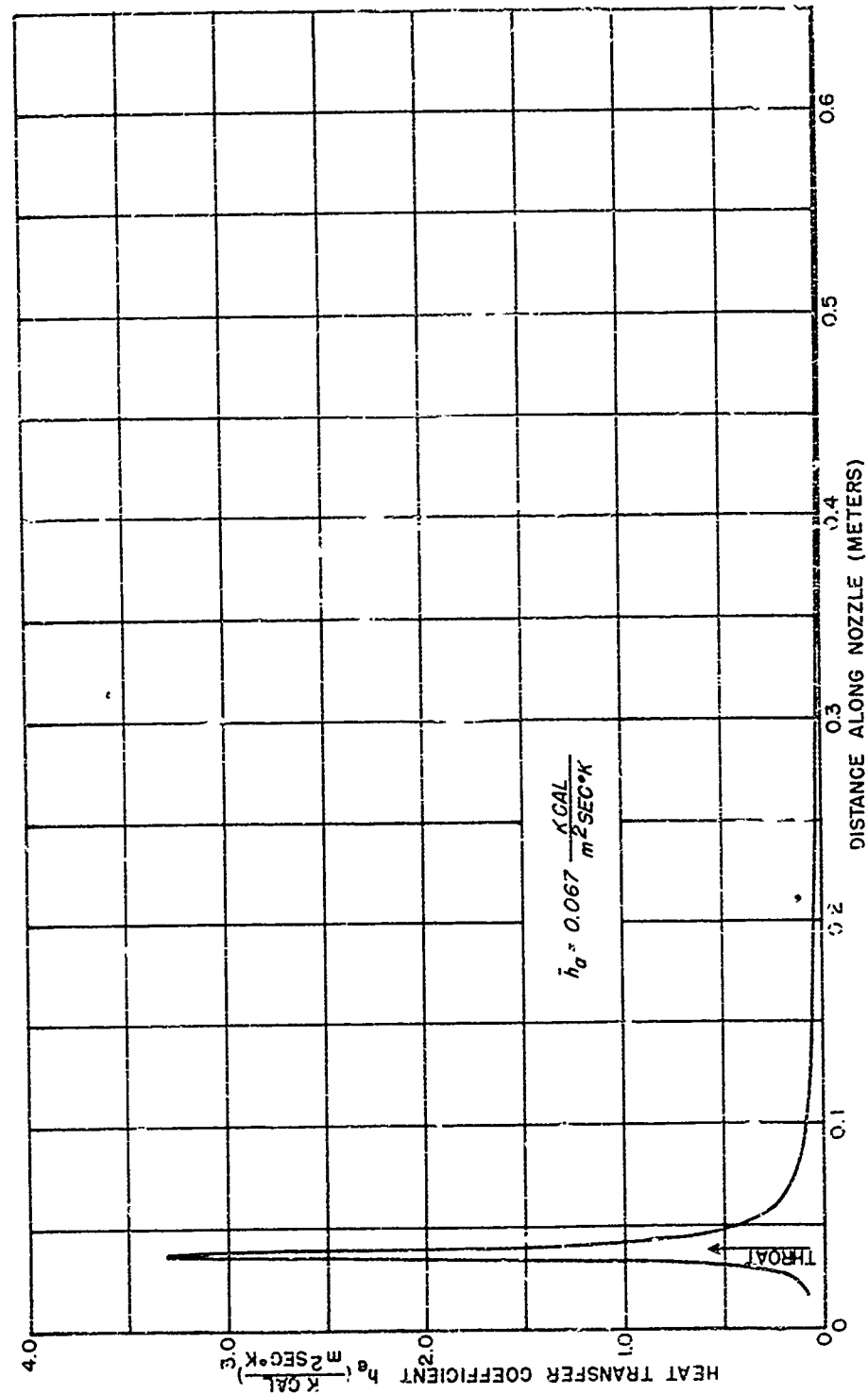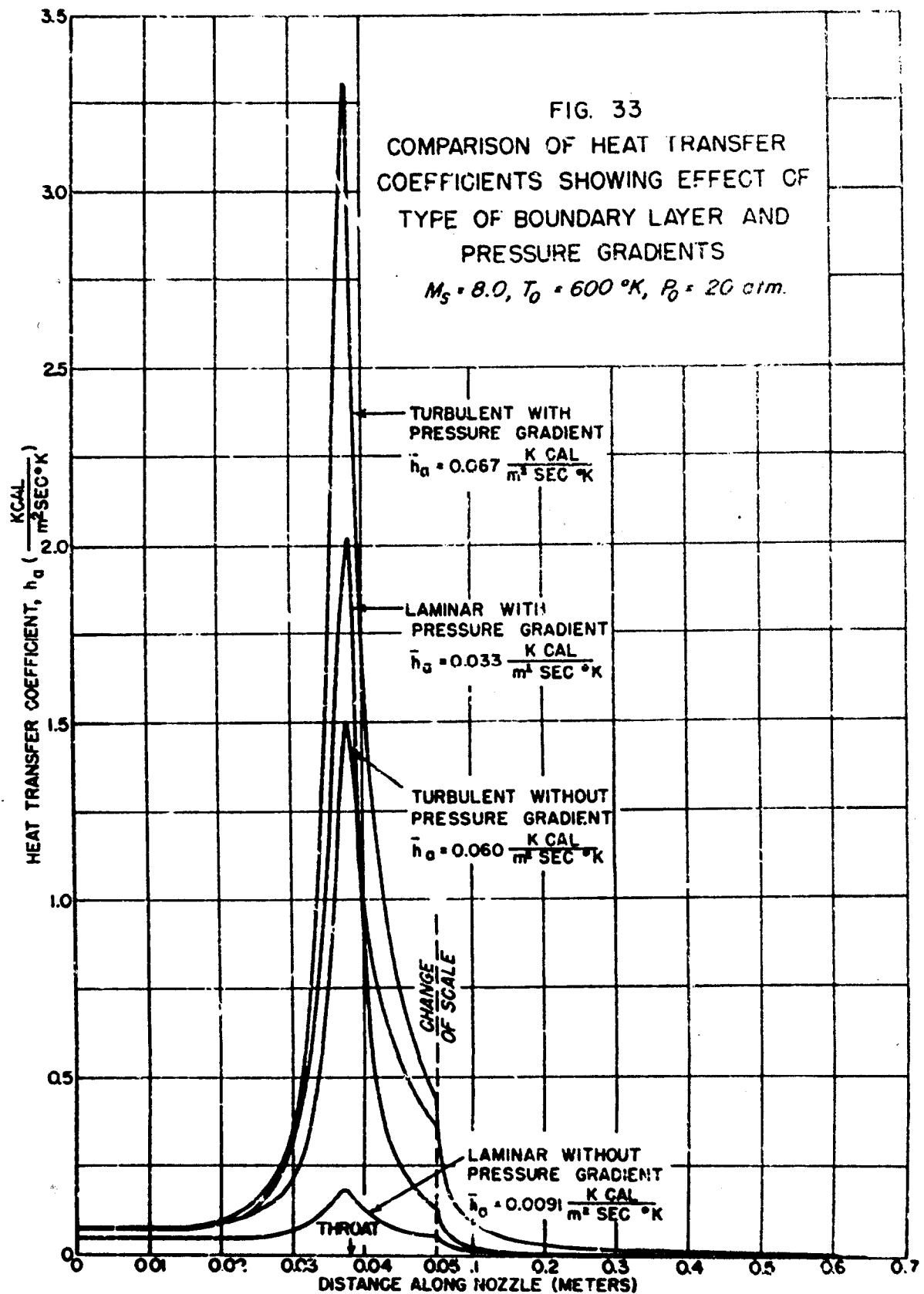$M_s = 8.0, T_o = 600°K, P_o = 20 atm$

FIG. 32   HEAT TRANSFER COEFFICIENT DISTRIBUTION ASSUMING TURBULENT FLOW
AND INCLUDING THE EFFECTS OF PRESSURE GRADIENTS
$M_s = 8.0, \; T_0 = 600\,°K, \; P_0 = 20\,atm$

FIG. 33
COMPARISON OF HEAT TRANSFER COEFFICIENTS SHOWING EFFECT OF TYPE OF BOUNDARY LAYER AND PRESSURE GRADIENTS
$M_S = 8.0$, $T_0 = 600\,°K$, $P_0 = 20\,atm.$

PLUG ROTATED 90° ON INSTALLATION SO THAT THERMOCOUPLE JUNCTIONS ARE POSITIONED FACING CENTER-LINE OF NOZZLE

IRON CONSTANTINE NO.30 GAGE WIRE 8 LEADS

THERMOCOUPLE EXTRACTOR BOLT

LOCK WASHER SLOT OPENING ENLARGED TO CLEAR WIRES

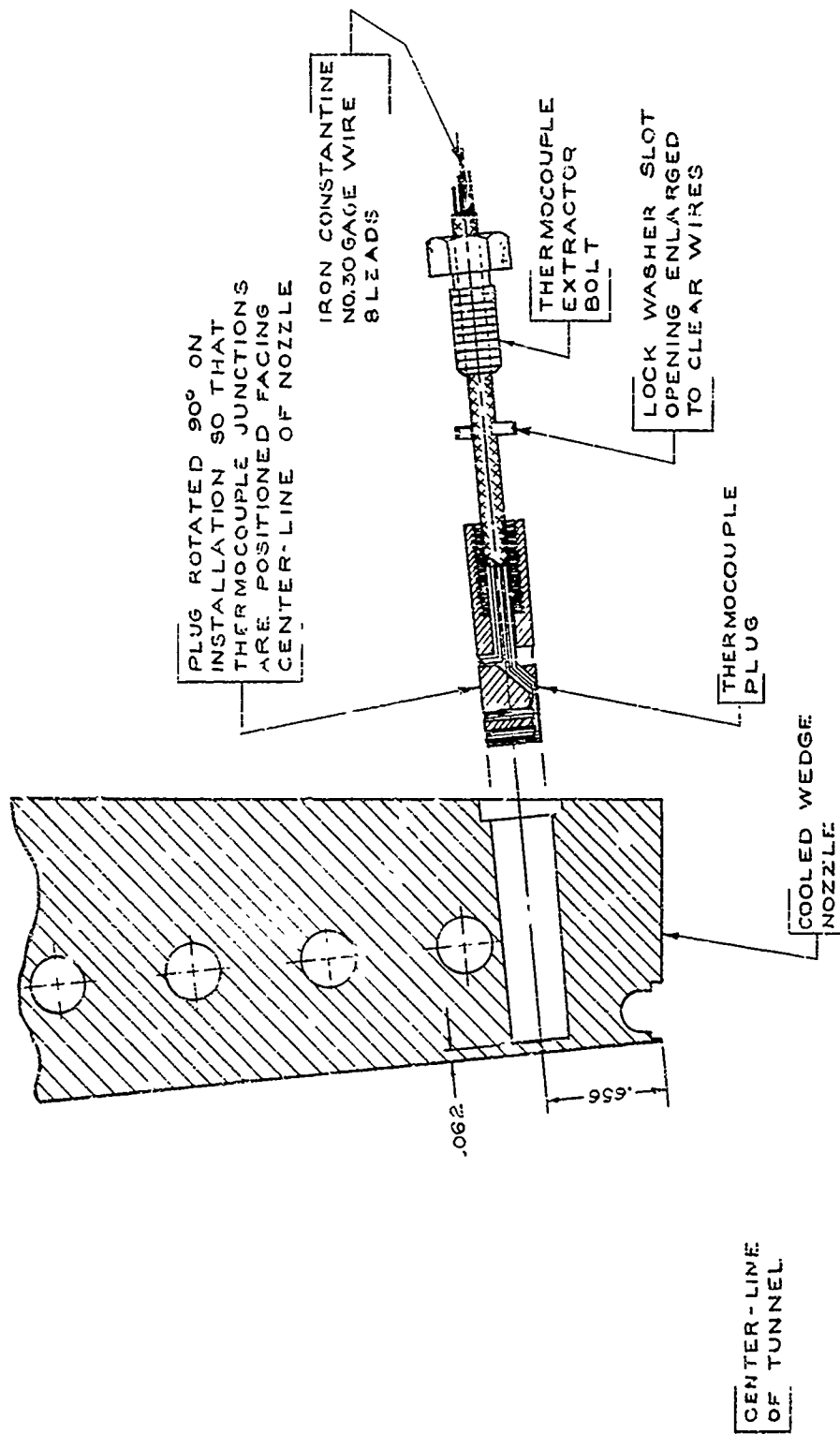THERMOCOUPLE PLUG

COOLED WEDGE NOZZLE

.062

.656

CENTER-LINE OF TUNNEL

FIG.-34 INSTALLATION OF THERMOCOUPLE PLUG IN NOZZLE BLOCK